Lineage-restricted regulation of SCD and fatty acid saturation by MITF controls melanoma phenotypic plasticity

Yurena Vivas-García[1,], Paola Falletta[1], Jana Liebing[2,3], Pakavarin Louphrasitthiphol[1,3], Yongmei Feng[4], Jagat Chauhan[1], David A Scott[4], Nicole Glodde[2], Ana Chocarro-Calvo[1,5], Sarah Bonham[6], Andrei L Osterman[4], Roman Fischer[6], Ze'ev Ronai[4], Custodia García-Jiménez[5], Michael Hölzel[2] and Colin R Goding[1,7]*

[1] Ludwig Institute for Cancer Research, Nuffield Department of Clinical Medicine, University of Oxford, Headington, Oxford, OX3 7DQ, UK.

[2] Institute of Experimental Oncology, University Hospital Bonn, University of Bonn, 53127 Bonn, GERMANY.

[4] Sanford Burnham Prebys Medical Discovery Institute, La Jolla, CA, 92037 USA

[5] Facultad de CC de la Salud, Edificio Dptal 1, Universidad Rey Juan Carlos, Avda Atenas s/n 28922, Alcorcón, Madrid. SPAIN

[6]Target Discovery Institute, Nuffield Department of Medicine, University of Oxford, Headington, Oxford, OX3 7FZ, UK

[7]Lead contact

[3]These authors contributed equally

*Correspondence: colin.goding@ludwig.ox.ac.uk

Running title: Melanoma plasticity and SCD

Summary
Phenotypic and metabolic heterogeneity within tumors is a major barrier to effective cancer therapy. Yet how metabolism is implicated in specific phenotypes, and whether lineage-restricted mechanisms control key metabolic vulnerabilities remains poorly understood. In melanoma, down-regulation of the lineage addiction oncogene Microphthalmia-associated Transcription Factor (MITF) is a hallmark of the proliferative-to-invasive phenotype switch, though how MITF promotes proliferation and suppresses invasion is poorly defined. Here we show that MITF is a lineage restricted activator of the key lipogenic enzyme stearoyl-CoA desaturase (SCD), and that SCD is required for $MITF^{High}$ melanoma cell proliferation. By contrast $MITF^{Low}$ cells are insensitive to SCD inhibition. Significantly, the MITF-SCD axis suppresses metastasis, inflammatory signaling, and an ATF4-mediated feedback-loop that maintains dedifferentiation. Our results reveal that MITF is a lineage-specific regulator of metabolic reprogramming, whereby fatty acid composition is a driver of melanoma phenotype-switching, and highlight that cell phenotype dictates response to drugs targeting lipid metabolism.

Key words: MITF/ATF4/Stearoyl CoA desaturase/Melanoma/Phenotype-switching/Fatty acid saturation

INTRODUCTION

A major barrier to effective cancer therapy is dynamic and reversible phenotype-switching of cells within tumors in response to a changing microenvironment (Brabletz et al., 2005; Marusyk and Polyak, 2010; Mlecnik et al., 2016; Nieto et al., 2016; Quail and Joyce, 2013). Since many therapies target proliferating cells, and other phenotypic sub-populations exhibit drug- and immunotherapy-resistance, understanding the mechanisms that promote inter-conversion between phenotypic states is a key issue.

An emerging theme is that different phenotypic states within a tumor will exhibit fundamentally different metabolic profiles (Jose et al., 2011). For example, hypoxia, one of the major microenvironments encountered by cells within tumors, induces a switch from oxidative phosphorylation toward glycolysis, known as the Pasteur effect (Marchiq and Pouyssegur, 2016). Moreover, highly proliferative BRAF-mutant melanomas are mainly dependent on glycolysis (Hall et al., 2013; Parmenter et al., 2014), whereas oxidative phosphorylation characterizes a sub-population of slow-cycling drug-resistant melanoma cells (Roesch et al., 2013; Zhang et al., 2016). It seems likely therefore that many of the hallmarks of specific phenotypic states within tumors are imposed via metabolic reprogramming. However, while the glycolytic-oxidative phosphorylation switches that drive cancer progression are well known, the importance of fatty acid metabolism has received less attention (Carracedo et al., 2013).

To support proliferation cancer cells require large amounts of saturated and monounsaturated fatty acids (SFA, MUFA) that are used for energy storage and production, membrane biogenesis and signaling (Currie et al., 2013). Consequently proliferating cancer cells can exhibit elevated expression of key enzymes required for de novo fatty acid synthesis including fatty acid synthase (FASN), ATP citrate lyase (ACLY) or stearoyl-CoA desaturase (SCD) that have been proposed as possible drug targets (Peck et al., 2016; Presler et al., 2018; Rysman et al., 2010; Ventura et al., 2015; Zaidi et al., 2012). However, although reprogramming lipid metabolism is an important characteristic of tumor cell biology, the molecular mechanisms underlying the transcriptional control of lipid anabolism in cancer cells remain underexplored.

The proportion of saturated and unsaturated fatty acids, is a crucial determinant of cell behavior (Currie et al., 2013), with the rate limiting step of fatty acid desaturation catalyzed by SCD (Koeberle et al., 2016). SCD is essential for proliferation in a wide variety of cancer types (Peck et al., 2016; Kamphorst et al., 2013; Pinkham et al., 2019; Presler et al., 2018; Xie et al., 2018; Igal, 2016). However, while *SCD* is regulated by Sterol Regulatory Element-Binding Protein (SREBP, SREBP1c, SREBF) (Tabor et al., 1999), a key transcription regulator implicated in lipid homeostasis (Shao and Espenshade, 2012), how SCD might be regulated in response to drivers of phenotypic plasticity in cancer is unknown.

Melanoma represents an excellent model to understand microenvironment-driven phenotype-switching (Rambow et al., 2019). Distinct mutually exclusive phenotypic sub-populations have been

observed within tumors (Goodall et al., 2008) and a key regulator of phenotypic plasticity identified (Hoek and Goding, 2010). The microphthalmia-associated transcription factor MITF (Goding and Arnheiter, 2019), a lineage survival oncogene (Garraway et al., 2005), up-regulates genes implicated in melanocyte differentiation (Carreira et al., 2005; Cheli et al., 2010), drives melanoma proliferation (Carreira et al., 2006; Garraway et al., 2005), and is down-regulated in invasive melanomas (Carreira et al., 2006). An $MITF^{Low}$ state is also associated with drug-resistance (Dugo et al., 2015; Konieczkowski et al., 2014; Muller et al., 2014; Rambow et al., 2018), and tumor-initiation capacity (Cheli et al., 2011). MITF presumably represses genes implicated in invasion (Strub et al., 2011), and activates those necessary for proliferation, a high nutrient-demand state. However, although MITF has been identified as a key regulator of mitobiogenesis via its regulation of Peroxisome Proliferator-activated Receptor Gamma Co-activator 1-alpha (*PGC1α, PPARGC1A*) (Haq et al., 2013; Vazquez et al., 2013) and controls the TCA cycle by regulating *SDHB* (Louphrasitthiphol et al., 2019), whether MITF regulates additional genes implicated in the metabolic rewiring that differentiates proliferative and invasive cells is not known.

RESULTS

SCD is suppressed by glutamine deprivation

In response to glutamine deprivation melanoma cells undergo a proliferative-to-invasive phenotype-switch characterized by de-differentiation and characteristics of drug- and immunotherapy-resistance (Falletta et al., 2017). Importantly, the phenotypic transition driven by low glutamine could be recapitulated by pharmacologically inducing translation reprogramming, characterized by phosphorylation of eIF2α, where global protein translation was attenuated, but expression of some proteins, including the stress-response transcription factor ATF4 was up-regulated (Falletta et al., 2017). Translation reprogramming down-regulated MITF expression both transcriptionally and translationally, leading to de-differentiation and invasion (Falletta et al 2017; Phung et al 2019). However, how MITF suppresses invasion and how translation reprogramming imposes the observed phenotypic and gene expression changes remains poorly understood.

To understand the consequences of translation reprogramming in melanoma we deprived IGR37 melanoma cells of glutamine for 4 h and 24 h, conditions that increased ATF4 protein expression and reduced MITF and protein translation (Figure S1) (Falletta et al., 2017), and used stable isotope labelling by amino acids in cell culture (SILAC) (Figure 1A) followed by liquid chromatography-mass spectrophotometry (LC-MS) to identify proteins whose translation was significantly altered. Interrogation of the differentially expressed proteins (Table S1) revealed that one of the most translationally down-regulated proteins in the two replicates was the fatty acid desaturase Stearoyl-CoA desaturase (SCD) (Figure 1B). We therefore focused our attention on the regulation of SCD expression, partly because the role of fatty acid saturation in melanoma biology is poorly understood,

and also because potent and selective SCD inhibitors are available. Notably SCD was even more down-regulated than MITF (Figure 1C). The down-regulation of SCD on glutamine deprivation was confirmed in three human melanoma cell lines by Western blotting (Figure 1D). No effect was observed on other key enzymes involved in fatty acid metabolism, such as ATP citrate lyase (ACLY), implicated in fatty acid synthesis, or carnitine palmitoyl transferase 1 (CPT1a), required for fatty acid oxidation (Figure 1E).

The differential expression of SCD detected using SILAC could arise either from down-regulation of its translation, its degradation or by suppression of its mRNA expression. Quantitative real-time RT PCR (qRT-PCR) (Figure 1F) revealed that low glutamine decreased SCD mRNA levels, but did not affect the expression of fatty acid synthase (FASN), with a decrease in *ACLY* mRNA expression also detected. Under the same conditions, an increase in ATF4 mRNA expression was observed, consistent with previous observations (Falletta et al., 2017).

We next used the glutamine starvation signature (GSS) derived from genes whose expression is altered after 6 h of glutamine deprivation (Falletta et al., 2017) to interrogate the TCGA melanoma cohort. Melanomas with a high GSS score exhibited an average low *SCD* mRNA expression (Figure 1G), suggesting that our findings in cell lines reflected regulation of *SCD* in tumors. Examination of the TCGA melanoma cohort, revealed that expression of several genes implicated in fatty acid metabolism differentially correlated with expression of *MITF*, a proliferative or invasive gene expression signature (Verfaillie et al., 2015), or *AXL*, a hallmark of a de-differentiated and drug-resistant phenotype (Dugo et al., 2015) (Figure S2A). Of these, *SCD* expression strongly positively correlated with that of *MITF* and the proliferative gene expression signature. Notably, the positive correlation between *SCD* and *MITF*/proliferative signature expression was even stronger in the Cancer Cell Line Encyclopedia (CCLE) melanoma gene expression data (Figure S2B). Ranking the TCGA melanoma cohort by *SCD* expression and interrogating each melanoma for a score corresponding to the expression of the Verfaillie invasive gene expression signature (Verfaillie et al., 2015) confirmed the strong anti-correlation between *SCD* mRNA and invasion in vivo (Figure S2C). Any correlation between *ACLY* or *FASN* expression with invasion was much less significant.

Knowing that de-differentiated and invasive melanomas are characterized by high *ATF4* and low *MITF* expression (Falletta et al., 2017), we deprived cells of glutamine and examined the relative expression of *SCD*, *ATF4* and *MITF* over time. The results (Figure 1H) revealed a strong downregulation of SCD protein accompanied by increased ATF4 expression followed by the expected decrease of MITF. In addition to amino acid deprivation, pseudo-starvation signals such as inflammation can also trigger translation reprogramming and melanoma dedifferentiation through TNFα signaling (Falletta et al., 2017; García-Jiménéz and Goding, 2019; Konieczkowski et al., 2014; Landsberg et al., 2012; Srivastava et al., 1998). We therefore treated IGR37 cells with TNFα and observed the expected down-regulation of MITF and SCD protein, accompanied by upregulation of

ATF4 and phosphorylation of the translation initiation factor eIF2α, an event that drives ATF4 protein translation (Figure 1I). The changes in MITF and SCD protein expression in response to TNFα were accompanied by reduced mRNA expression (Figure S2D).

Translation reprogramming represses SCD expression

To investigate the possibility that translation reprogramming and ATF4 could regulate SCD transcription and translation, we treated IGR37 melanoma cells with salubrinal, which inhibits dephosphorylation of eIF2α (Boyce et al., 2005). Salubrinal treatment of melanoma increases p-eIF2α, decreases global translation, up-regulates expression of ATF4, decreases transcription and translation of MITF, and promotes melanoma invasion and tumor initiation capacity (Falletta et al., 2017). Consistent with translation reprogramming suppressing SCD and MITF expression, salubrinal repressed SCD and MITF protein levels (Figure 2A). Moreover, salubrinal-mediated down-regulation of SCD was also observed at the mRNA level, as was the repression of *MITF* and induction of *ATF4* (Figure 2B). No repression of *CPT1a* was observed, suggesting again an exclusive effect on *SCD* regulation.

Using cell lines engineered to express doxycycline-inducible ATF4 in a stress-independent manner (Falletta et al., 2017), induction of ATF4 using doxycycline robustly repressed *SCD* expression at the protein (Figure 2C) and mRNA (Figure 2D) levels, with no significant effect on *ACLY* (Figure 2C) or *FASN* (Figure 2D) expression. These data were confirmed using immunofluorescence in which SCD protein was detected only in cells within the population that did not induce ATF4 (Figure 2E). Of note, SCD expression was decreased even in those cells expressing ATF4 to a low level (Figure 2E, enhanced red channel).

***SCD* is a direct target of MITF**

The results so far indicate that translation reprogramming and ATF4 induction in response to glutamine limitation, TNFα or salubrinal can down-regulate *SCD*. However, chromatin-immunoprecipitation followed by high-throughput sequencing (ChIP-seq) failed to identify ATF4 bound in the vicinity of the *SCD* gene, while binding to known ATF4 targets was readily observed (data not shown) suggesting that ATF4 mediated suppression of *SCD* is indirect. One possibility was that MITF can also regulate *SCD* and that ATF4 would regulate *SCD* indirectly via its ability to suppress MITF expression. This would be consistent with the strong correlation between *SCD* and *MITF* expression in the TCGA melanoma cohort (Figure 3A), and RNA-seq analysis of a panel of melanoma cell lines comprising both $MITF^{High}/AXL^{Low}$ (proliferative) and $MITF^{Low}/AXL^{High}$ (invasive) lines (Figure 3B). The MITF-negative, SREBP-high breast cancer cell line HBL-100 was used as a control. The high correlation between *MITF* and *SCD* mRNA in the melanoma cell lines was confirmed by western blotting, with SCD protein being poorly expressed in $MITF^{Low}$ cells (Figure

3C). Using a 501mel melanoma cells line stably expressing ectopic MITF under a doxycycline-inducible promoter, 24 h after doxycycline stimulation we observed a moderate, but significant, up-regulation of *SCD* mRNA to a similar extent as *PCG1α* (Figure S3A), a validated MITF target gene (Haq et al., 2013; Vazquez et al., 2013). By contrast, a robust down-regulation of *SCD* expression was achieved at both protein and mRNA levels using siRNA-mediated depletion of MITF in 3 melanoma cell lines, using *PGC1α* and *CPT1a* as controls (Figure 3D). These results were confirmed using a second independent siRNA targeting MITF (Figure S3B). Chromatin-immunoprecipitation followed by high-throughput sequencing (ChIP-seq) revealed MITF binding at both the 5' and 3' ends of the SCD gene (Figure 3E), suggesting that the regulation of *SCD* by MITF was direct.

The ability of MITF to regulate directly *SCD* would be consistent with the observed repression of *SCD* by ATF4 being linked to the ability of ATF4 to silence *MITF* expression, as previously described (Falletta et al., 2017; Ferguson et al., 2017). To test this we used cells transiently overexpressing ATF4 in which MITF could be induced using doxycycline (Figure 3F, left and middle panels) and examined the effects on *SCD* mRNA expression. The results (Figure 3F, right panel) indicated that while ATF4 overexpression alone could repress *SCD* mRNA levels (also Figure 2D), and MITF induction alone could induce *SCD* (Figure S3A), the repression of *SCD* by ATF4 could be reversed on MITF expression. To ensure that any of the changes in SCD expression observed were not due to an effect of doxycycline itself, we treated parental cells with the same dose of doxycycline (100 ng/mL), and as expected, no significant effect was observed at the mRNA or protein level on SCD, ATF4 or MITF (Figure S3C).

Since SCD activity controls the SFA/MUFA ratio, we used GC-MS to analyze the fatty acid profiles of the $MITF^{High}/SCD^{High}$ BRAF mutant IGR37 cell line, and its $MITF^{Low}/SCD^{Low}$ IGR39 counterpart isolated from the same patient. The results revealed that $MITF^{Low}$ IGR39 cells exhibited an increased ratio of C16:0 saturated to C16:1 mono-unsaturated long chain fatty acids (Figure 3G), consistent with the low SCD expression in these cells (Figure 3B, C). The high C16:0 to C16:1 fatty acid ratio observed in the $MITF^{Low}/SCD^{Low}$ IGR39 cells compared to the $MITF^{High}/SCD^{High}$ IGR37 cells was recapitulated by siRNA-mediated MITF knockdown using two different siRNAs in 501mel cells, though no change was observed in the ratio of C18:0 to C18:1 fatty acids (Figure 3H, Figure S3D). Similar results were also obtained following salubrinal treatment of IGR37 cells (Figure S3E), or following exposure of cells to TNFα (Figure S3F), conditions that also down regulate SCD expression (Figure 1I, Figure 2A,B). Collectively the results suggest that MITF controls melanoma fatty acid composition through regulation of SCD expression.

An MITF-SCD feedback loop controls protein synthesis

Consistent with SCD playing a key role in fatty acid desaturation in SCD-positive melanoma cells, the treatment of IGR37 cells with the SCD inhibitor A939572 increased SFA levels compared to

MUFAs, with cells exhibiting a substantial increase in 16:0 palmitic acid and 18:0 stearic acid, and a decrease in palmitoleic acid (16:1) (Figure 4A). By contrast, in the $MITF^{Low}/SCD^{Low}$ IGR39 cell line the SCD inhibitor had no significant impact on fatty acid composition (Figure S4A). Changes in the balance of SFA:MUFAs can affect the composition and biophysical properties of cell membranes and induce endoplasmic reticulum stress (ER-stress) and the Unfolded Protein Response (UPR) by affecting the dimerization of PERK and IRE1 within the lipid bilayer (Volmer and Ron, 2015; Volmer et al., 2013). Consistent with this, siRNA-mediated SCD depletion, or inhibition of SCD using A939572, led to ER-stress characterized by alterations in XBP1 splicing (Figure 4B) and increased XBP1s mRNA expression (Figure S4B, C). The expression of the ER-chaperone BiP, a key marker of UPR, was also increased on SCD inhibition (Figure S4D). SCD inhibition using two different inhibitors (A939572 and CAY10566) to minimise off target effects, or siRNA-mediated SCD depletion also increased ATF4 expression and decreased MITF (Figure 4C), consistent with SCD activity suppressing ER-stress and the UPR. The effect of SCD inhibition on ATF4 and MITF protein, was reflected in a moderate up-regulation of *ATF4* and repression of *MITF* mRNA (Figure S4B, C), as well as induction of the ATF4 target *CHOP* (*DDIT3*) (Figure S4C). Although ATF4 expression may be controlled transcriptionally, it is primarily regulated by translation dependent on eIF2α phosphorylation (Harding et al., 2000). Consistent with the induction of ATF4 protein, eIF2α phosphorylation was induced by SCD inhibition, an effect abrogated by addition of oleic acid, a C18:1 monounsaturated fatty acid (Figure 4D). Elevated phosphorylation of eIF2α (Figure 4D) after SCD inhibition coincided with a mobility shift in the ER-stress-activated kinase PERK (Figure S4E), indicating its activation by phosphorylation as a consequence of SCD inhibition triggering ER-stress. We detected no effect of SCD inhibition or depletion on the expression of the MITF regulator BRN2 indicating that the effects observed on ATF4 and MITF were specific (Figure S4F). SCD inhibition also suppressed phosphorylation of the mTORC1 targets 4EBP1 (marked by a mobility shift) and S6K (Figure S4G). The inhibition of mTORC1 signaling by SCD inhibition could be attributed to up-regulation of the ATF4 target gene *SESTRIN 2* (*SESN2*) (Ye et al., 2015) (Figure S4H), a known repressor of mTORC1 (Byun et al., 2017; Kim et al., 2015; Wolfson et al., 2016).

Consistent with SCD inhibition inducing eIF2α phosphorylation and inhibiting mTORC1 signaling, SCD inhibition, or depletion using two different siRNAs, led to decreased incorporation of ^{35}S-methionine into newly translated protein (Figure 4E). Taken together, the results suggest that SCD and the degree of fatty acid saturation may drive phenotype-switching in melanoma by reprogramming translation leading to ATF4 activation, repression of MITF transcriptionally and translationally, and consequently induce melanoma de-differentiation. Importantly, decreased SCD expression or activity will impose a positive feedback loop in which increased ATF4 and decreased MITF will further reduce SCD expression, thereby stabilizing the $MITF^{Low}$ de-differentiated phenotype.

Cell phenotype dictates response to SCD inhibitors

Unlike normal cells, cancer cells exhibit an increased capacity for de novo fatty acid synthesis which fulfills the high demand for lipid associated with elevated proliferation rates (Carracedo et al., 2013). Indeed, many tumors express high levels of enzymes involved in fatty acid synthesis, including SCD (Peck et al., 2016). Whether high SCD is a hallmark of proliferating melanomas is unknown. We therefore interrogated the TCGA melanoma cohort and found a strong positive correlation between SCD mRNA expression and the Verfaillie proliferative signature gene set (Verfaillie et al., 2015), especially in those melanomas with the lowest SCD expression (Figure 5A). Since SCD in melanoma also correlates with MITF (Figure 3A) and anti-correlates with the Verfaillie invasive gene expression signature (Figure S2C), these data suggest that cells with low SCD activity would be de-differentiated, invasive and slow-cycling. As such, clinical use of SCD inhibitors would be expected primarily to target proliferating cells, as has been proposed in studies showing that SCD inhibitors can prevent proliferation of breast and prostate cancer cells in culture (Peck et al., 2016). We therefore treated four human melanoma cells lines with the SCD inhibitor A939572. Remarkably the inhibitor prevented proliferation of the $MITF^{High}$ IGR37 and 501mel cell lines (Figure 5B, C), and as observed in other cell types (Peck et al., 2016), moderately increased apoptosis indicated by caspase3/7 staining (Figure 5D) and cleaved PARP1 (Figure 5E). By contrast, inhibition of SCD had little effect on the $MITF^{Low}$ lines IGR39 or A375M (Figure 5B, C). The effect of SCD inhibition on IGR37 and 501mel cells was reversed by addition of the C18:1 MUFA oleic acid (Figure 5B, C). Differential effects of SCD inhibition on proliferation were also observed using mouse melanoma cell lines previously characterized for MITF expression (Riesenberg et al., 2015); $MITF^{High}$ HCmel12 cells were substantially more sensitive to SCD inhibition than the $MITF^{Low}$ HCmel10 cells (Figure S5A, B).

SCD inhibition in $MITF^{High}$ melanoma cells turned off expression of MITF (Figure 5F), a lineage addiction oncogene that drives proliferation via suppression of the $p27^{Kip1}$ (CDKN1B) cyclin-dependent kinase inhibitor and activation of *CDK2* expression (Carreira et al., 2006; Du et al., 2004; Garraway et al., 2005). SCD inhibition also down regulated E2F1 (Figure 5F), a cell cycle regulator fundamental for melanoma survival, proliferation and metastasis formation (Dar et al., 2011; Ghosh et al., 2005; Halaban et al., 2000; Pandolfi et al., 2015; Riverso et al., 2017; Rouaud et al., 2018). The effects of SCD inhibition on both transcription factors were largely reversed by addition of oleic acid (Figure 5F) or oleic acid (C18:1) together with palmitoleic acid, a C16:1 monounsaturated fatty acid (Figure S5C), to complement the lack of SCD activity. Notably E2F1 expression was dependent on MITF (Figure 5G), with MITF binding upstream from the E2F1 promoter detected using ChIP-seq (Figure 5H). Thus at least in part, the effects of SCD and MUFAs on proliferation are likely to be via MITF, including MITF-mediated regulation of E2F1.

Consistent with the differential effect of SCD inhibition on the $MITF^{High}$ and $MITF^{Low}$ cell lines, the SCD inhibitor A939572 substantially increased the SFA:MUFA ratio in the sensitive IGR37 cell

line, but only moderately in the insensitive IGR39 cell line (Figure 5I). An imbalance in fatty acid composition, such as that induced by SCD inhibition in the MITF-positive IGR37 cells, should, in addition to supressing MITF expression, activate autophagy, a survival response associated with the UPR (B'Chir et al., 2013; Bernales et al., 2006) in which cells recycle unnecessary organelles in order to restore an imbalance in nutrient supply and demand (Rzymski et al., 2009). In agreement with this, SCD inhibition induced an increase in the LC3II isoform in $MITF^{High}$ (501mel, IGR37) melanoma cells, as reported in other cells types (Janikiewicz et al., 2015; Ogasawara et al., 2014; Peck et al., 2016), but did not increase autophagy in the $MITF^{Low}$ (IGR39, A375M) cell lines (Figure 5J).

SCD suppresses inflammation and dedifferentiation.

Given the key role of SCD in maintaining an MITF-positive proliferative phenotype, we assessed the genome-wide impact of SCD inhibition. Two MITF-positive SCD inhibitor-sensitive cell lines, IGR37 and 501mel, were analyzed by RNA-seq 48 h after transfection with control, or two SCD-specific siRNAs. SCD inhibition led to a similar pattern of up- and down-regulation of genes in the two cell lines (Figure 6A; Figure S6A; Tables S2, S3, S4). The results were recapitulated using the SCD inhibitor A939572 in IGR37 cells (Figure S6B; Table S5). Following SCD depletion or inhibition, Gene Set Enrichment Analysis (GSEA) (Figure 6A; Figure S6A-C) revealed a strong decrease in expression of genes implicated in cell cycle progression (E2F and MYC targets), consistent with the reduced proliferation in SCD-inhibited MITF-positive melanoma cell lines (Figure 5B,C; Figure S5A,B) and low MITF-dependent E2F1 expression in response to SCD inhibition (Figure 5F-H; Figure S5C). In agreement with SCD inhibition leading to apoptosis (Figure 5 D,E), the RNA-seq analysis confirmed the upregulation of Hallmark Apoptosis genes.

In the RNA-seq dataset, several key biological processes were enriched including strong up-regulation of the unfolded protein response (UPR) (consistent with PERK activation) (Figure S4E), up-regulation of ATF4 and eIF2α phosphorylation (Figure 4), the p53 pathway and increased expression of genes associated with an epithelial-to-mesenchymal transition (EMT) (Figure S6C). This reflected a moderate increase in invasion in a matrigel assay following SCD inhibition in IGR37 cells (Figure S6D), and a marked increase in invasion and speed of migration through collagen (Figure 6B). We also noted elevated expression of the EMT-associated protein fibronectin (FN1) (Figure 6C), and AXL (Figure 6D) associated with an $MITF^{Low}$ drug-resistance phenotype (Dugo et al., 2015; Konieczkowski et al., 2014; Muller et al., 2014; Rambow et al., 2018).

The RNA-seq analysis (Figure 6A; Figure S6A-C) also revealed a substantial increase in TNFα-driven NFκB-mediated inflammatory signalling, confirmed using two different SCD-specific siRNAs that both increased expression from an NFκB-dependent luciferase reporter (Figure 6E). siRNA-mediated depletion or inhibition of SCD reduced expression of the NFκB inhibitor IκBa (Figure 6F). Consistent with these observations, qRT-PCR confirmed that SCD inhibition increased inflammatory

cytokine gene expression (Figure 6G), as well as IL6 and IL8 secretion (Figure 6H) and intracellular accumulation (Figure S6E). Depletion of the p65 NFκB subunit largely prevented the increased cytokine expression observed on SCD inhibition using A939572 (Figure S6F), and also diminished the increase in ATF4 expression observed following exposure to A939572 concomitant with MITF downregulation (Figure 6I).

Notably, the eIF2α phosphatase inhibitor salubrinal, reduced levels of the short-lived IκBa inhibitor of NFκB (Figure S6G) and consequently activated an NFκB-dependent luciferase reporter (Figure S6H), in agreement with previous observations (Deng et al., 2004). Salubrinal also inhibited both MITF and SCD expression and induced ATF4 (Figure 2A, B; Figure S6G). These observations are consistent with ER-stress induced following SCD inhibition resulting in the activation of NFκB signaling and inflammatory gene expression. However, although activation of NFκB in response to reduced SCD activity may account in part for the increased cytokine expression observed, elevated ATF4, arising as a consequence of the UPR induced by SCD inhibition (Figure 4B-D; Figure 6A; Figure S4B-E), was also likely to contribute since ATF4 can drive inflammatory gene expression (Gargalovic et al., 2006; Huang et al., 2015; Zhang et al., 2013). Consistent with this, cytokine gene expression increased after doxycycline treatment of a melanoma cell line (Falletta et al., 2017) engineered to express inducible ATF4 (Figure S6I).

The main transcriptional changes described in human melanoma cells were also induced by pharmacological inhibition (CAY10566) of SCD in two mouse melanoma cell lines, HCmel12 and B16F1, indicating that SCD regulates melanoma cell plasticity in different species (Figure S7; Table S6).

SCD inhibition promotes inflammation and metastatic dissemination *in vivo*.

To establish the role and regulation of SCD in melanomas *in vivo*, we used three complementary models based on mouse cell lines so as to preserve an intact immune system in the host.

First, we used MITF-positive B16-F1 melanoma cells, which respond to SCD inhibition in a similar way to human cells (Figure S7C). Cells were injected subcutaneously and after 13 days (when tumors reached 3-5 mm in diameter) mice were injected intraperitoneally with the A939572 SCD inhibitor (twice per day for 5 days) before the tumors were removed and mRNA extracted for RNA-seq analysis. GSEA analysis of the results (Figure 7A) indicated similar gene expression changes to those observed in human or B16 melanoma cells *in vitro* (Figure S7C). Namely strong up-regulation of inflammatory signaling and apoptosis and E2F and MYC targets. We also noted that two fatty acid carrier proteins, SLC27A1/FATP1 and CD36 previously involved in melanoma survival and metastasis initiation (Pascual et al., 2016; Zhang et al., 2018) were strongly up-regulated (Figure 7B), presumably to facilitate uptake of monounsaturated fatty acids to complement the inhibition of SCD. However, although this model is useful, the rapid growth of the B16-F1 tumor model does not allow

us to monitor metastatic dissemination, given the need to terminate the experiment in accord with animal welfare. Therefore to determine the effects of SCD inhibition on metastasis we used the SW1 model of NRAS mutated melanoma; when injected subcutaneously SW1 tumors grow more slowly than those obtained using B16-F1 cells, and disseminate widely, including to the lungs. As with the human melanoma cell lines, SW1 cells in culture respond to SCD inhibition by phosphorylating eIF2α, up-regulating ATF4 and downregulating MITF (Figure 7C). SW1 cells were therefore inoculated subcutaneously and after 1 week mice were either treated with vehicle only (Group 1), with A939572 SCD inhibitor twice daily for 9 days before treatment was halted (Group 2), or treated first for 9 days, and again from day 12-16 and at days 19 and 20 (Group 3) (Figure 7D). For all three groups tumor volumes were measured for 20 days post-treatment. Note that for Group 2 we chose the 9 day treatment followed by a drug holiday until day 20 since we were unsure how effectively SCD inhibition would affect melanoma proliferation *in vivo*; if it were very effective it might promote invasion and dissemination but block proliferation and tumor expansion of the lung metastases, preventing us from determining the effect on metastasis.

The results (Figure 7E) revealed that for both groups treated with the SCD inhibitor, primary tumors grew less rapidly than those given vehicle alone although the effects were mild. However, SCD inhibition promoted a substantial increase in lung metastases (Figure 7F), consistent with the results in human melanoma cell lines showing SCD inhibition increased invasion (Figure 6B). Moreover, MITF was downregulated in the primary tumors of the mice in Group 3 (Figure 7G), in agreement with the increased number of metastases found in this group. In Group 2 MITF levels were not down-regulated at the 20 day endpoint, perhaps reflecting the 11 day drug holiday at the end of the treatment period during which MITF levels could recover.

Finally, we used a previously established mouse model of inflammation-driven resistance to adoptive T-cell therapy (Landsberg et al., 2012; Reinhardt et al., 2017) to examine SCD expression early and late during therapy. In this model (Figure 7H) HCmel3 melanoma cells are injected subcutaneously and mice are treated with cytotoxic T-cells engineered to target the melanoma differentiation antigen Pmel/Gp100. In response to the T-cell therapy, tumors initially regress, but then relapse and are resistant to the therapy as a consequence of TNFα-mediated dedifferentiation associated with loss of Pmel/gp100 antigen expression (Landsberg et al., 2012; Reinhardt et al., 2017). Gene expression analysis of the untreated tumors (NT), those early during treatment (EDT), or those after relapse (R), confirmed by GSEA analysis that TNFα signaling was elevated in both EDT and relapse (Figure 7H), and revealed that *Scd1* expression decreased significantly during early treatment and remained low during relapse (Figure 7I). We also observed the expected decrease in Mitf expression and upregulation of Atf4 and its canonical target Asns. This result reflects *in vivo* the ATF4/MITF/SCD axis that we have shown *in vitro* (Figures 2-4). The expression of Ppargc1a (PGC1α), a target of both Mitf (Haq et al., 2013; Vazquez et al., 2013) as well as Srebp (Hao et al.,

2010), followed that of Mitf and was suppressed both early during treatment and after relapse, suggesting that this gene is primarily regulated by Mitf in melanoma (Figure 7I). We also noted that, consistent with the results of the B16-F1 tumors, expression of the fatty acid transporter *Slc27a1* was decreased early during treatment, but recovered during relapse. Although the differential expression of *Slc27a1* was not statistically significant, the trend does suggest a possible compensatory response when cells are faced with a reduction in SCD expression.

DISCUSSION

Although MITF coordinates melanocyte and melanoma biology by integrating inputs from the tumor microenvironment to promote proliferation and suppress invasion, whether and how MITF coordinates the cell cycle with availability of building blocks necessary for cell growth was unclear. Our results provide three insights into how MITF activity can establish and maintain specific melanoma phenotypic subpopulations through regulation of melanoma metabolism. First, we identify MITF as a lineage-restricted regulator of *SCD* and fatty acid saturation; second, we show that low SCD activity promotes translation reprogramming, inflammatory signaling and reduced MITF expression, thereby establishing a positive feedback loop to stabilize an $MITF^{Low}$ state linked to increased metastatic dissemination; and third, we show that $MITF^{High}$ but not $MITF^{Low}$ melanoma cells are sensitive to SCD inhibition, meaning that phenotypic heterogeneity within tumors poses a major barrier to effective SCD inhibitor-based therapy.

Previous work established that *SCD* is regulated by SREBP (Tabor et al., 1999) and PPAR transcription factors (Kim et al., 2000), thereby coordinating the supply of MUFAs with intracellular sterol levels. However, in cancer *de novo* fatty acid synthesis may not be fully dependent on SREBP (Williams et al., 2013). For example in Burkitt's lymphoma XBP1s activates SCD expression in a context of high MYC, (Xie et al., JCI, 2018) while desaturases in ovarian stem cells are regulated by NFκB (Li et al., 2017). However, the existence of cell type-specific regulators has not been previously established. Here we identify MITF as a key lineage-restricted alternative regulator of *SCD*. Consistent with this, MITF-positive cell lines express low levels of SREBP mRNA, suggesting that in these cells the main regulator of MUFA synthesis is MITF.

Uncoupling long chain fatty acid biosynthesis from desaturation can affect breast and glioblastoma cell proliferation and viability (Peck et al., 2016; Williams et al., 2013). Consistent with this, inhibition or depletion of SCD in MITF-positive melanoma cells prevents proliferation and promotes apoptosis that can be prevented by addition of oleic acid. Thus, by regulating *SCD*, MITF acts as a lineage addiction oncogene in melanoma by enabling cells to generate the MUFAs necessary for cell growth and division. Moreover, changes in fatty acid composition have a direct impact on MITF expression and its target gene *E2F1*, strongly suggesting that the effects of MUFAs on melanoma proliferation are at least partially mediated by their effect on MITF levels.

The inflammatory gene expression observed on SCD inhibition arises as a consequence of p-eIF2α-mediated translation reprogramming which activates NFκB by preventing synthesis of the short-lived NFκB inhibitor IκB (Deng et al., 2004; Ferreiro and Komives, 2010; Tam et al., 2012), and ATF4 that drives expression of cytokines such as IL-8, IL-6 or CCl2 (Gargalovic et al., 2006; Huang et al., 2015). Translation reprogramming can suppress MITF mRNA expression via ATF4 (Falletta et al., 2017; Ferguson et al., 2017), but also decreases MITF translation (Falletta et al., 2017). This then leads to low SCD mRNA expression which in turn triggers ER-stress, eIF2α phosphorylation, and activation of inflammatory ATF4 and NFκB signaling. Thus, low SCD activity activates a positive feedback loop (Figure 7J) that reinforces and maintains an $MITF^{Low}$ dedifferentiated state. Importantly, an $MITF^{Low}/NF\kappa B^{High}$ profile is associated with resistance to BRAF inhibitors and is linked high expression of *AXL* (Konieczkowski et al., 2014; Muller et al., 2014). Low SCD activity increases ATF4 and NFκB signalling, both of which can drive AXL expression and BRAF/MEK inhibitor-resistance (Falletta et al., 2017; Konieczkowski et al., 2014). Our results showing SCD blockade leads to an $MITF^{Low}/AXL^{High}$ state is therefore consistent with the suggestion that changing fatty acid composition may confer resistance to anticancer therapy (Cai et al., 2016; Iwamoto et al., 2018).

We also note that in the adoptive T-cell mouse model, where resistance is associated with de-differentiation mediated by TNFα signaling and NFκB activation (Landsberg et al., 2012), Scd and Mitf mRNA expression were suppressed. This is consistent with inflammatory signaling via NFκB participating in a positive feedback loop to maintain an $Mitf^{Low}/Scd^{Low}$ state; TNFα suppresses Mitf and Scd protein expression through translation reprogramming, while low Scd activity drives inflammatory signaling. The regulation of *SCD* primarily by MITF, and potentially by SREBP, and NF-κB (Li et al., 2017), endows melanoma cells with considerable flexibility in their response to the intratumor microenvironment. Although in Burkitt's lymphoma SCD is regulated by the spliced isoform of X-box binding protein 1 (XBP1s) that is activated by ER-stress (Xie et al., 2018), we have not observed regulation of *SCD* by XBP1s in melanoma. Most likely XBP1s-mediated regulation of *SCD* may be restricted to cells in which ER-stress is chronic.

Previous work has identified SCD as a potential target for therapy in several cancer types (Fritz et al., 2010; Mason et al., 2012; Peck et al., 2016; von Roemeling et al., 2013), including melanoma (Pisanu et al, 2018). However, previous studies did take into account the impact of the microenvironment in generating phenotypic heterogeneity; MITF-positive cell lines exhibit an exquisite sensitivity to SCD inhibition, but $MITF^{Low}$ melanoma cells are largely insensitive. It seems plausible therefore that $MITF^{Low}$ cells may depend on uptake of fatty acids from their environment, consistent with the fatty acid transporter CD36 playing a key role in successful metastatic outgrowth (Pascual et al., 2016. Ladanyi, 2018 #6413) and the alternative fatty acid transporter, FATP1/SLC27A1 being essential for melanoma progression (Zhang et al., 2018). Indeed in B16 tumors *in vivo*, we show SCD inhibition increases CD36 and FATP1/SLC27A1 expression that

presumably confer increased fatty acid uptake in the face of an inability to synthesize MUFAs. These observations pose a particular challenge to any SCD inhibitor-based anti-cancer therapy. Although some cancer cells can upregulate the alternative desaturase FADS2 when SCD is inhibited (Vriens et al., 2019), inhibition of SCD in a clinical setting may drive some cells to activate the positive feedback loop identified here that would increase de-differentiation, invasion, metastatic capacity, AXL-associated drug-resistance and inflammatory signaling. Consistent with this, SCD inhibition enhances cell invasion *in vitro* and substantially increased lung metastasis *in vivo*. In agreement, invasive B16F10 melanoma cells exhibit low membrane MUFA content compared to the non-invasive B16F1 variant (Schroeder and Gardiner, 1984). For SCD inhibitors to be effective, it is likely that combination therapies will be needed, for example by blocking both fatty acid uptake as well as SCD, or by applying directed phenotype-switching (Saez-Ayala et al., 2013) to drive de-differentiated melanoma cells to turn on MITF and up-regulate SCD.

To conclude, our results identify *MITF* as a novel regulator of fatty acid desaturation and suggest the MITF-SCD axis is a critical determinant of melanoma phenotypic identity.

ACKNOWLEDGMENTS

Funding was provided by the Ludwig Institute for Cancer Research (CRG, PL), The NIHR Oxford Biomedical Research Centre (JC), NIH grant PO1 CA128814-06A1 (PF, YVG, DAS, ALO, YF, ZR, CRG), NIH Cancer Center grant P30 CA030199 supporting the SBP Cancer Metabolism Core (DAS), a European Union Marie Curie FP7-PEOPLE: PIEF-GA-2013-626098 and EMBO Long-Term Fellowship: ALTF 800–2013, Comunidad de Madrid, Ayudas Atracción de Talento 2017-T1/BMD-5334 (AC-C), Spanish government Grant Nos. PI13/01150, SAF2016-79837-R and Universidad Rey Juan Carlos-Banco de Santander (Grupo Excelencia QUINANOAP) (CG-J), and The Kennedy Trust (RF) and DFG Excellence Cluster ImmunoSensation^2 (EXC2151) (MH). Mass spectrometry analysis was performed in the TDI MS laboratory led by Benedikt M. Kessler.

AUTHOR CONTRIBUTION

YVG, PF, YL, YF, AC-C, , CG-J and CRG conceived the experiments, AO and DS undertook fatty acid analysis, SB and RF performed the Mass Spec analysis. PL and JC undertook bioinformatics analyses. JL, NG and MH performed tumorigenesis assays and mouse mRNA expression analysis. ZR, CG-J, MH and CRG provided supervision. YVG and CRG wrote the manuscript.

DECLARATION OF INTERESTS

The authors declare no competing interests

Figure 1. SCD is suppressed by glutamine starvation

(A) SILAC mass spectrometry approach to identifying proteins differentially expressed after 4 h or 24 h glutamine (Q) starvation. Light R0K0, Medium R6K4 and Heavy R10K8 media used to label the cells are described in the STAR Methods. See also Figure S1

(B) Expression ratios of 5885 quantified proteins (all SILAC channels) in both replicates for the 4 h or 24 h glutamine starvation vs un-starved condition. MITF (yellow) and SCD (green) expression are highlighted. The blue area represents 90% of the data density. See also Table S1.

(C) Differential expression of MITF and SCD proteins after 4 or 24 h glutamine starvation.

(D) Western blot of indicated melanoma cell lines grown in MEM with 2 or 0.1 mM glutamine probed with indicated antibodies. ERK or Tubulin were loading controls.

(E) Western blot of IGR37 melanoma cells grown in 0.1 mM glutamine probed with indicated antibodies. ERK was a loading control.

(F) RT qPCR for indicated genes grown in DMEM or MEM + 2 mM or 0.1 mM glutamine for 24 or 48 h.** p <0.01; *** p <0.001; **** p <0.0001. Error bars represent mean +/- SEM.

(G) The 471 melanomas in the TCGA cohort were ranked by SCD expression (black line). Grey bars indicate average expression of the 103 genes comprising the GSS in each tumor. The blue line represents the moving average of the GSS over each 20 tumors.

(H) Western blots of cell lines grown in 0.1 mM glutamine probed with ATF4, MITF and SCD antibodies. GAPDH was a loading control.

(I) Western blots of IGR37 melanoma cells treated with 50 ng/mL TNFα probed with indicated antibodies. GAPDH was a loading control. See also Figure S2D

Figure 2. Translational reprogramming and ATF4 repress SCD expression

(A) Western blot of IGR37 or 501mel cells grown in the absence or presence of 50 μM Salubrinal. ERK was a loading control.

(B) RT qPCR for indicated genes from IGR37 cells grown with or without 50 μM Salubrinal. * p <0.05; ** p <0.01. Error bars represent mean +/- SEM.

(C) Western blot for indicated genes in 501mel or SKmel28 melanoma cells expressing doxycycline-inducible ATF4 (iATF4). Cells were grown +/- 100 ng/ml doxycycline. Tubulin was a loading control.

(D) RT qPCR for indicated genes in Skmel28 iATF4 cells grown in the presence of 100 ng/ml doxycycline for indicated times. * p <0.05; ** p <0.01; *** p <0.001. Error bars represent mean +/- SEM.

(E) Immunofluorescence of SKmel28-iATF4 or B16-iATF4 cells grown for 24 h +/- 100 ng/ml doxycycline as indicated. SCD (green) and ATF4-expressing cells (red) are indicated. Arrows

indicate cells in which ATF4 was not induced and SCD expression is maintained. Scale bar = 20 μm.

Figure 3. SCD expression is controlled by MITF

(A) The 471 TCGA melanomas were ranked by expression of *SCD* (black line). Grey bars indicate average expression of *MITF* in each tumor, and brown line represents the moving average of *MITF* expression over each 20 tumors.

(B) Heatmap of relative expression of indicated genes from triplicate 3'RNA-seq across indicated cell lines.

(C) Western blot of indicated melanoma cell lines. Tubulin was a loading control.

(D) RT qPCR for indicated genes and western blot for MITF and SCD in melanoma cell lines 72 h after transfection with control or MITF-specific siRNA. ** p <0.01. Error bars represent mean +/- SEM. See also Figure S3B.

(E) Biological replicate MITF ChIP-seq showing MITF occupancy at the *SCD* gene.

(F) RT qPCR for ATF4, MITF and SCD mRNA in response to exogenous ATF4 or MITF overexpression. ** p <0.01; *** p <0.001; **** p <0.0001. Error bars represent mean +/- SEM. See also Figure S3C.

(G) GS-MS analysis showing ratio of saturated and monounsaturated fatty acids in IGR37 and IGR39 cells. ** p <0.01. Error bars represent mean +/- SEM. See also Figure S3D-F.

(H) GS-MS analysis showing ration of saturated to monounsaturated fatty acids in 501mel cells following transfection with control of MITF-specific siRNA. * p<0.05. Error bars are +/- SEM. See also Figure S3D-F.

Figure 4. Identification of an ATF4-SCD-MITF feedback loop

(A) GS-MS analysis showing total fatty acid content of IGR37 cells +/- treatment with 1 μM A939572 SCD inhibitor for 48 h. * p < 0.05. Error bars represent mean +/- SEM. See also Figure S4A.

(B) RT PCR for XBP1 splice isoforms in IGR37 cells treated with SCD specific siRNA or 1μM A939572 SCD inhibitor. H: hybrid from unspliced and spliced XBP1 isoforms; u: unspliced XBP1; s: spliced XBP1. See also Figure S4B-E.

(C) Western blot of IGR37 or 501mel cells showing ATF4 and MITF expression after SCD inhibition using 1 μM A939572 or 100 nM CAY10566, or transfection with SCD-specific siRNAs for 48 h. GAPDH or ERK were loading control.s See also Figure S4F.

(D) Western blot of IGR37 or 501mel cells showing phospho-eIF2α and eIF2α expression after SCD inhibition using 1 μM A939572, +/- of 100 μM oleic acid (18C:1). GAPDH was a loading control.

(E) Coomassie staining or ^{35}S-methionine incorporation into IGR37 or 501mel cells treated with 1 μM A939572 or depleted of SCD using different siRNAs.

Figure 5. Phenotype-specific dependency on SCD

(A) 471 melanomas in the TCGA cohort were ranked by *SCD* expression (black line). Grey bars indicate average expression in each tumor of genes comprising the Verfaillie Proliferative signature. Brown line represents the moving average of the Proliferative signature over each 20 tumors.

(B) Indicated cell lines were grown for 120 h in a 12 well plate +/- 1 μM A939572 or 100 μM of oleic acid as indicated before crystal violet staining. See also Figure S5A,B.

(C) Proliferation of indicated cell lines grown +/- 1 μM A939572 or 100 μM of oleic acid as indicated. Quantification obtained by 0.1% crystal violet staining of three independent experiments. Data presented as mean ± SEM. Statistics show differences between different treatments at each specific time point. * $p < 0.05$; ** $p < 0.01$

(D) Apoptosis assays using cleaved anti-caspase 3/7 antibody to identify the apoptotic population by flow cytometry 72 h after treatment with A939572 1 μM in the MITF^{High} melanoma cells IGR37 and 501mel. Data presented as mean ± SEM of 5 biological replicates. **** *p*-value<0.0001

(E) Western blot for PARP and PARPc of indicated cell lines treated with 1 μM A939572. GAPDH was a loading control.

(F) Western blot of IGR37 cells showing MITF and E2F1 expression after treatment with 1 μM A939572, +/- 100 μM oleic acid (18C:1). TUBULIN was a loading control. See also Figure S5C.

(G) Western blot for MITF and E2F1 in melanoma cell lines transfected for 72 h with control or MITF-specific siRNAs 72 h. GAPDH was used as loading control.

(H) Biological replicate MITF ChIP-seq showing MITF occupancy at the *E2F1* gene.

(I) GS-MS analysis showing ratios of saturated and monounsaturated fatty acids in IGR37 and IGR39 melanoma cells treated with 1 μM A939572 for 48 h. Data presented as mean ± SEM. ** $p < 0.01$; *** $p < 0.001$

(J) Western blot for LC3 of cells grown in the absence or presence of 1 μM A939572 or 100 nM CAY10566 for 72 h. TUBULIN was a loading control.

Figure 6. SCD promotes cell proliferation and suppresses inflammatory signaling and invasion

(A) Heatmaps and GSEA analyses derived from 3' RNA-seq of IGR37 or 501mel cells depleted for SCD using a specific siRNA (siSCD#1) for 48 h. See also Tables S2-S5. See also Figure S6A-C.

(B) 3D migration collagen assays performed using 501mel and IGR37 melanoma cells. Results presented as mean ± SEM of 5 or 6 biological replicates. * $p < 0.05$; ** $p < 0.01$. See also Figure S6D.

(C) Western blot for FN1 of 501mel or IGR37 cells treated with 1 μM A939572 or 100 nM CAY10566 for 5 days. GAPDH was a loading control.

(D) Western blot using anti-AXL antibody of IGR37 and 501mel cells treated with 1 μM A939572 or 100 nM CAY10566 for 5 days. TUBULIN was used as a loading control.

(E) Luciferase assay and western blot of IGR37 or 501mel cells transfected with SCD-specific siRNAs for 48 h together with an NFκB-dependent promoter-luciferase reporter. * $p < 0.05$; ** $p < 0.01$, *** $p < 0.001$; **** $p < 0.0001$

(F) Western blots showing IκBa levels after SCD inhibition or siRNA-mediated knockdown.

(G) RT qPCR for indicated genes from 501mel or IGR37 cells treated with 1 μM A939572 for 48 h or 72 h as indicated. Data represent mean ± SEM. * $p < 0.05$; ** $p < 0.01$, *** $p < 0.001$; **** $p < 0.0001$. See also Figure S6E, F.

(H) IL-8, IL-6, and CXCL1 levels in media of 501mel and IGR37 cells treated with 1 μM A939572 at indicated times. Data represent mean ± SEM of 5 to 8 biological replicates. * $p < 0.05$; ** $p < 0.01$, *** $p < 0.001$; **** $p < 0.0001$.

(I) Western blot for phospho-eIF2α, eIF2α, ATF4 and MITF of IGR37 is 501mel cells treated as indicated with A939572 and transfected with control or p65 (NFκB)-specific siRNA. GAPDH was is a loading control.

Figure 7. SCD inhibition in vivo induces inflammation dedifferentiation and metastasis

(A) GSEA analysis of B16 cell primary tumor 3'RNA-seq from mice treated either with vehicle or A939572 SCD inhibitor (dose: 25 mg/kg).

(B) Gene expression values for the fatty acid importers SLC27A1, SLC27A3, SLC27A4, SLC27A6 and CD36 obtained from the 3'RNA-seq of B16 cells primary tumors from mice treated either with vehicle or A939572 SCD inhibitor.

(C) Western blot for phospho-eIF2α, eIF2α, ATF4, MITF and SCD of SW1 mice cells treated in vitro with 1 μM A939572. TUBULIN is a loading control.

(D) Schematic showing the SW1 mouse experiments. 3 groups were established (n=10 mice/group): GROUP 1 (treated with vehicle); GROUP 2 (treated for 9 days, twice per day with A939572); GROUP 3 (treated for 16 days, twice per day with A939572). The red arrows

indicate the days when A939572 was administrated (IP, Dose: 25 mg/kg). D=day. All samples were collected at D 20.

(E) SW1 primary tumor volumes from mice treated with either vehicle, SCD inhibitor during 9 days or SCD inhibitor for 16 days. N=10 mice/group. Error bars represent mean +/- S.E.M.

(F) Images of lung sections SW1 primary tumors treated or not with A939572 as indicated time. The table shows the number of metastases observed in numbers of lungs.

(G) Western blot for MITF of SW1 primary tumors from mice treated or not with A939572 for the indicated time. GAPDH is a loading control.

(H) Schematic showing the mouse experiment using HCmel3 cells treated with cytotoxic T-cells targeting the melanoma differentiation antigen Pmel/Gp100. GROUP 1 (Non treated (NT); n=8); GROUP 2 (early during treatment (EDT); n=13); GROUP 3 (Relapse (R); n=5). Primary tumors were collected and analyzed by RNA-seq.

(I) Box plots showing the relative expression of the indicated genes from microarrays of untreated (UT), early during treatment (EDT) or relapsed (R) mouse melanomas after T-cell immunotherapy. Box plot horizontal lines and whiskers indicate quartiles. * $p < 0.05$; ** $p < 0.01$; *** $p < 0.001$, **** $p < 0.0001$ unpaired two-sided *t*-test with Benjamini and Hochberg correction.

(J) The MITF-SCD axis in melanoma.

STAR METHODS

LEAD CONTACT AND MATERIALS AVAILABILITY

Materials Availability Statement: Further information and requests for resources and reagents should be directed to and will be fulfilled by the Lead Contact, Colin R Goding (colin.goding@ludwig.ox.ac.uk).

METHOD DETAILS

Melanoma cell line panels

Human cell lines (IGR37, IGR39, 501mel, A375M, SKmel30.1, SKmel28, WM852, HBL, HBL-100) and murine cell lines (B16, HCmel10, HCmel12, HCmel3, SW1) were cultured in 5% CO2 at 37°C with 1% penicillin–streptomycin in RPMI plus 10% fetal bovine serum (FBS) or in DMEM or MEM with 10% dialyzed FBS. Where indicated, MEM was supplemented with 42 mg/L 0.4 mM serine, 30 mg/L 0.4 mM glycine, and glutamine at 2 or 0.1 mM. Inducible cell lines were derived as described previously (Falletta et al., 2017) using the doxycycline-inducible Piggybac system in which the Piggybac transpon is used to integrate Tet-on activator expression vector and the Tet-regulated cDNA of interest. All the cell lines were tested monthly for mycoplasma using MycoAlert™ mycoplasma detection kit (Lonza) and authenticated using short tandem repeat (STR) profiling.

Stable isotope labelling with amino acids in cell culture (SILAC) for Liquid Chromatography Tandem Mass Spectrometry (LC-MS/MS)

IGR37 melanoma cells were grown in SILAC DMEM (Invitrogen) supplemented with 10% dialysed FBS (Biosera), 1000 mg/ml Glucose (Sigma), Glutamine 4 mM (Thermo), 1% penicillin/streptomycin (Sigma). 73 mg/l of Lysine and 126 mg/l Arginine were added to the medium to prepare the different populations of labelled cells: Light R0K0, Medium R6K4 and Heavy R10K8. Specifically, R0K0 Light medium was supplemented with Arginine Hydrochloride and Lysine Hydrochloride. R6K4 medium was supplemented with K4 (L-Lysine-4,4,5,5-d4 hydrochloride) and R6 (L-Arginine-13C6 hydrochloride) and R10K8 Heavy medium was supplemented with K8 (L-Lysine-13C6,15N2 hydrochloride) and R10 (L-Arginine-13C6,15N4 hydrochloride). All amino acids were purchased from Sigma Aldrich. The two cell populations were grown in corresponding culture medium for 15 cell doublings by changing medium every 2 days. The glutamine starvation experiment was performed in a biological duplicate with labels switched. Each population of cells, R0K0 (Light), R6K4 (Medium) and R10K8 (Heavy), was plated in 2 sub-confluent T175 flasks and starved for glutamine for either 4 h or 24 h or not starved. Glutamine starvation medium was prepared as described for the stable isotope labelling without the addition of Glutamine which was normally present at 4 mM. The 6 samples obtained were lysed in RIPA Lysis Buffer (20 mM Tris-HCl pH 7.5, 150 mM NaCl, 1 mM EGTA 1% NP-40 1% sodium dehoxycholate, protease and phosphatase inhibitors (Roche)), protein

concentration was measured with bicinchoninic acid (BCA) according to standard protocols and Trypsin digested. After protein concentration normalization, samples were mixed to obtain two batches containing the different times of glutamine starvation in a forward/reverse labelling scheme: Batch 1: R0K0 24h Q starved, R6K4 not starved, R10K8 4 h Q starved; Batch 2: R0K0 4h Q starved, R6K4 24h Q starved, R10K8-not starved. To increase proteome depth, samples were pre-fractionated using high pH fractionation into 45 fractions per sample and analyzed as 15 concatenates as described earlier (Davis et al., 2017). The 2 batches were analyzed by LC-MS/MS at the Target Discovery Institute (Oxford) on an Orbitrap Fusion Lumos platform. Data was analyzed with Maxquant (V. 1.6.2.2 (Cox and Mann, 2008)) using default settings in addition to the "match between runs option", followed by visualisation in Perseus (Tyanova et al., 2016). Quantitation results are available in suppl. Table S1 and have been deposited with protein identifications and raw files in the PRIDE data repository (Vizcaino et al., 2016) under the accession PXD010254.

Western blot

Whole-cell protein lysates were subjected to 7.5 or 10% polyacrylamide SDS- PAGE. Proteins were transferred onto nitrocellulose membranes (Amersham Biosciences). Membranes were blocked with 5% nonfat milk in PBS containing 0.1% Tween 20 and probed with the appropriate primary antibodies (see Key Resources Table) overnight at 4°C. Proteins were detected using anti-mouse or anti-rabbit immunoglobulin coupled to horseradish peroxidase (Bio-Rad and Santa Cruz Biotechnology) and visualized with an ECL detection kit (Amersham Biosciences). A minimum of three different experiments were done in each case.

RT-qPCR

Total RNA was extracted from 3 replicates of melanoma cells using the RNeasy minikit (Qiagen). Reverse transcription of 0.5-1 µg of RNA was performed according to the manufacturer's instructions using the QuantiTect reverse transcription kit (Qiagen). Primers for human genes were designed using the Primer Blast application from NCBI (see Key resources table). Reactions were performed in SYBR Green mix (Go-Taq, Promega) and analyzed using a Corbett Rotor-Gene 6000. Melting curve analyses were carried out to ensure product specificity, and to calculate the relative quantity of gene expression, a standard curve method was performed. Relative mRNA expression levels were normalized to ß-2-microglobulin. Three biological replicates were included in each experiment and the data were represented as mean ± SEM.

Immunofluorescence microscopy

Engineered doxycycline-inducible mCherry-P2A-ATF4 cells (Falletta et al., 2017) or parental cells were grown with and without doxycycline (100 ng/ml) on 100 mm^2 coverslips, fixed in 4%

paraformaldehyde, permeabilized and blocked with 0.2% Triton X-100, 5% BSA in PBS for 20 min and probed with the appropriate antibody (see Key Resources Table) for 20 min at room temperature. In the inducible cells, SCD was detected with fluorochrome-conjugated secondary antibody Alexa-488, and mCherry (ATF4) was detected by using 546 nm channel. In the parental cells, SCD was detected with fluorochrome-conjugated secondary antibody Alexa-488, MITF with fluorochrome-conjugated secondary antibody Alexa-488 or Alexa-546 and ATF4 using fluorochrome-conjugated secondary antibody Alexa-546. Images were captured with an LSM 710 confocal microscope (Carl Zeiss), and processed with Adobe Photoshop CS6 (Adobe Systems).

TCGA and CCLE transcriptomic analysis

RNA-seq data from the TGCA melanoma cohort was accessed following the TCGA guidelines (http://cancergenome.nih.gov/publications/publicationguidelines) using the R-based CGDS-(Verfaillie et al., 2015) as has the glutamine starvation signature (GSS) (Falletta et al., 2017). For individual genes of interest or averaged signatures the moving average expression was calculated using a sample window size of n=20. Trendlines were added to the barplots and an R-skript for calculating and generating moving average plots of TCGA cancer cohorts implementing TCGA access via cBioportal was described previously (Riesenberg et al., 2015) was determined by An asymptotic Spearman correlation test using the original log2 expression values and not the moving average values, was used to determine The significance of the Spearman rank correlation.

ChIP-Seq analysis

Duplicate ChIP experiments were performed as described in Louphrasitthiphol et al. (2019), with each replicate containing two technical replicates, that were stitched together using UNIX to generate a single fastq. FastQCed was used to check the read quality or the Raw fastq files and PCR duplication, were processed and then mapped to the human genome build hg19 (GRCh37, February 2009) allowing for 2 mismatches using Bowtie. For peak calling mapped SAM-files were used in the Homer package. HA antibody against 501mel parental cell lines was used in a control ChIP-seq to generate background files. Using the Homer package peaks were assigned to the nearest gene and filtered for those with a peak score >10. Data presented in this manuscript correspond to data sets previously reported in Louphrasitthiphol et al. (2019).

RNAi gene Silencing

Silencing experiments were performed in triplicate, using two different specific siRNAs (20 nM) against MITF or SCD, and a negative control siRNA (See Key Resources Table). Cells were cultured in RPMI without antibiotic and transfected using OptiMem solution and Lipofectamine RNAiMAX (Invitrogen). Cells were collected after 48 h or 72 h after transfection.

RNA-seq of human melanoma cell lines *in vitro* and B16-F1 mouse cells *in vivo*

Using the RNeasy mini kit total RNA (Qiagen) was extracted from IGR37 and 501mel cells in which SCD had been silencing using two different siRNAs (see Key resources table) or inactivated by adding the specific inhibitor A939372 at 1 uM for 48 h. RNA quality was checked using a Bioanalyzer (for RIN ≥9.5) and 3 μg were used to perform sequencing. ERCC ExFold RNA Spike-In Mixes (Ambion) was added prior to Library prep using QuantSeq Forward kit (LEXOGEN #015.96), using 500 ng starting material to minimise the PCR amplification step. Samples prepared as biological triplicates were sequenced on HiSeq 2500 (Illumina) carried out using the Wellcome Trust genomic service, Oxford.

The output raw fastq files were trimmed of poly-A using Cutadapt (Martin, 2011) and mapped using STAR(Dobin et al., 2013) against hg38 (GRCh38, 2015). Counts per gene from STAR were used as input for differential gene expression analysis using EdgeR (Robinson et al., 2010). Reads for each sample set were first filtered for genes whose expression is <1 count-per-million prior to glmQLFTest. Genes with a p-value ≤0.05 and meet the specific fold-changes were taken for further analysis. Heatmaps of RNA-seq samples were generated from the edgeR-library normalised reads of genes whose differential gene expression has p-value ≤0.05 before further filtering for genes with read counts ≥2 counts in all the replicates of either treated or control samples. Raw reads were log2 transformed, centered normalised around mean and hierarchical clustering performed using complete linkage using Gene Cluster 3.0 (de Hoon et al., 2004). The output matrix was used to generate the heat-map for visualisation using TreeView (Saldanha, 2004). GSEA analyses were carried out using javaGSEA2-3.0 (Subramanian et al., 2005). 10,000 permutations were carried out for each RNA-seq geneset, using gene expression data from IGR37 and 501mel samples untreated or treated with the SCD inhibitor A9939572 (1 μM) or two different siRNAs against SCD was performed. The GSEA analysis for the *in vivo* experiment was performed as for the *in vitro* experiments except the pre-ranked data (-log10(PValue)/sign(logFC)) was used as input.

RNA-seq of mouse melanoma cells *in vitro*

Experiments were performed in biological triplicates. HCmel12 or B16F1 cells were treated with 100 nM CAY10566 for 72 hours or vehicle (DMSO). Cells were lysed in 200 μl RLT buffer (Qiagen) and total RNA was isolated using Zymo I spin columns (Zymo Research) and eluted in 8 μl of RNAase-free H_2O. RNA concentrations were determined using Qubit (LifeTech). 3' mRNA-seq library preparation was performed using the forward QuantSeq 3'mRNA-Seq Library Prep Kit for Illumina (Lexogen GmbH, Austria) according to the manufacturer's protocol. Size distribution and yield of the 3' mRNA-seq library after the PCR step was determined by the D1000 high sensitivity tape station (Agilent) prior to pooling of the barcoded libraries. The pooled 3' mRNA-Seq libraries were loaded on the Illumina HiSeq2500 platform and analyzed by a 50 cycles high-output run (UKB NGS core

facility, Bonn). Raw data will be available through GEO (SRA) archive. Computational 3' mRNA-seq analysis was done with the Bioconductor/R computing environment. FASTQ files were aligned to the mm10 mouse reference genome using the RSubread aligner package. The voom method of the limma package was used for normalization and linear modeling. mRNA expression values were transformed to log2 values of read counts per million.

Lipid extraction and fatty acid composition analysis

Samples in triplicates from control 501mel cells or cells depleted using siRNAs for MITF, and IGR37 and IGR39 cells treated for 48 h with the SCD inhibitor A939572 (1 uM), Salubrinal (50 uM) or for 96 h with TNFα (50 ng/mL) were collected. A minimum of two experiments were performed per condition, and three replicates were included in each individual experiment.

Cells were grown in 6-well plates in RPMI to a final density of $\geq 4 \times 10^5$ cells per well. Culture medium was removed and cells were washed quickly three times with cold PBS. Methanol/ water (1:1 mixture by volume, 0.45 ml,-20°C) was added and culture plates were placed on dry ice for 30 min, then thawed on ice for 10 min. A cell scraper was used to detach any cells still attached to the plate and the cell suspension/ extracts were transferred to micro-centrifuge tubes. Chloroform (0.225 ml) containing 4 µg/ml heptadecanoic acid as internal standard was added, tubes were vortexed briefly twice, and centrifuged for 5 min at 12,000 g 4°C. The bottom layer (chloroform extract) was transferred to separate tubes and dried in a centrifugal evaporator. Blank samples from wells without cells were prepared by the same procedure to control for any contaminating environmental fatty acids. The samples were stored at -80°C until use. The fatty acid content in the non-polar fraction was quantified by using GC-MS.

Fatty acids were derivatized with 50 µl 0.5 N HCl in methanol (Sigma), heated for 30 min at 60 °C with shaking at 850 rpm, dried by centrifugal evaporation, and resuspended in 50 µl pyridine (with heating at 60 °C) before transfer to GC-MS vials.

Samples were run on a Shimadzu QP2010 Plus GC-MS fitted with a 15 m x 0.25 mm x 0.25 µm RXI-5ms (Restek). Injection volume was 1 µl with a 1/10 split ratio and an injection temperature of 250°C. The GC oven temperature was initially 80°C for 3.5 min, rising to 280°C at 10°C/min with a final hold at this temperature for 2 min. The helium carrier gas flow rate was 50 cm/s. GC-MS interface temperature was 300°C and (electron impact) ion source temperature 200°C, with 70 eV ionization voltage. The mass spectrometer was set to scan m/z range 100-500 (starting at 3.5 min). In parallel with samples, serial dilutions of a mixture of 37 fatty acid methyl esters (Sigma FAMES-37 mix) were run as standards. Results from standards were used to construct calibration curves in MetaQuant (Bunk et al., 2006). Quantities of fatty acids in samples were determined in MetaQuant using these calibrations, and corrected for recovery of the internal standard (heptadecanoic acid).

^{35}S-methionine labeling

Cells seeded on 6 cm plates were treated with the SCD inhibitor A939572 (1uM) or transfected with two different siRNAs against SCD. After 48 h, 250 μCi/ml [^{35}S]-methionine/cysteine Express Protein Labeling mix (Perkin Elmer) was added to the media. After 20 min incubation, cells were washed twice in ice-cold PBS and lysed in 500 μL of lysis buffer (10 mM Tris at pH 7.5, 50 mM NaCl, 0.5% NP-40, 0.5% deoxycholate, 0.5% SDS) supplemented with protease inhibitors. Twelve microliters of each lysate was removed, analyzed by SDS-PAGE, and visualized by Coomassie staining and phosphorimager analysis to determinate the protein synthesis rate.

Crystal violet staining and cell density quantification

For the human cell lines, 25,000 cells were plated in a 12-well plate and treated with DMSO, A939572 (1 uM), or with A939572 (1 uM) and oleic acid (100 uM) simultaneously over 96 hours or 120 hours as indicated. Plates were collected at time 0, 24, 72, 96 or 120 h, fixed with 4% PFA and stained with 0.1% crystal violet for 15-30 min. Then they were washed, dried and scanned with a Fuji FLA-5100 imager. Quantification of the crystal violet intensity was made using ImageJ.

For the mouse cell lines, 5,000 cells (HCmel10 or HCmel12) were plated at low density in 12-well plates and treated with A939572 or CAY10566 at indicated concentrations or DMSO for 6 days. Cells were washed with PBS, fixed in 4% formaldehyde solution and stained with 0.1% crystal violet for 30 min. Then they were washed, dried and scanned and quantified using the Odyssey SA Infrared Imaging System (LICOR Biosciences).

Apoptosis by Caspase-3/7 Green flow cytometry assay

IGR37 and 501mel cells at 60%–70% of confluency were treated with the SCD inhibitor A939572 (1 uM) during 72 h. After this time cells were collected and apoptosis was analyzed using CellEvent Caspase-3/7 Green flow cytometry assay kit (C10427 Thermofisher), according to manufacturer's instructions. 10,000 cells were measured by FACS on a BD FACSCanto II (BD Biosciences), and data were analyzed using FlowJo software (7.6.1). 5 different experiments were performed for each cell line.

Matrigel invasion assays

Matrigel invasion assays were performed using invasion chambers from BD Biocoat. 30,000 cells previously treated during 24 h with DMSO or SCD inhibitor A939572 (1 μM) were seeded per insert and cultured in medium without FBS overnight. Medium with FBS was added to the bottom of the inserts. After incubation, cells remaining above the insert membrane were removed by gentle scraping with a sterile cotton swab. Cells that had invaded through the Matrigel to the bottom of the insert were fixed in ethanol for 15 min, washed in phosphate-buffered saline (PBS), and stained with crystal violet to be counted. Cells were manually counted using Image J software. Four biological replicates were performed.

3D collagen migration assays

Cells previously treated or not with SCD inhibitor A939572 (1 μM) were stained during 30 min with 5 μg/ml Hoechst 33258 and 20000 of those cells were re suspended in 200 μl of serum-free bovine collagen I at 2.3 mg/ml, previously prepared according to supplier instructions. Cells mixed with collagen, containing or not SCD inhibitor, were seeded on 8-well chambered cover-glass slides (Lab-Tek, cat#155411), centrifuged at 1100 rpm for 15 minutes at 4° to prevent gelation, and later chambers were maintained during 3 h at 37° to allow collagen gel formation. To ensure all cells were located at the coverslip, a z-stack line scan was taken using the reflection of the coverslip. Then, 10% FBS-containing media was added on top of the gel, allowing the cells to invade upwards for 24 h. After this time, cells were fixed in 4% PFA for 3 h and stained with DAPI. Chambered cover-glass slides were imaged using a LSM 710 confocal microscope (Carl Zeiss), with a Plan Apochromat 10x/0.30 objective and Zen Black software. Confocal z-slices were collected from each well at the bottom coverslip and at different levels along the collagen thickness (2000 μm max. height) and images of DAPI fluorescence and DIC were recorded simultaneously to ensure complete cell visualization and counting. The migration percentage was calculated as number of observed invading cells divided by the total number of cells. Distance in migration was calculated based on differences between the bottom position and other z-stack positions where cells were found. A total of 5 to 6 different biological replicates were performed per condition.

NF-κB reporter Luciferase activity

IGR37 and 501mel melanoma cells where SCD was silenced, or treated with salubrinal (50 μM), were co-transfected, using FuGENE6 (Promega), with 100 ng of NF-KB luciferase reporter construct pBIIXluc and with 100 ng of thymidine kinase-renilla luciferase construct for normalization of transfection efficiency. Forty-eight hours after transfection, cells were lysed, and luciferase activity was measured in triplicate using the luciferase reporter kit (Promega) and ClarioStar Multidetection system. A minimum of 5 experiments were performed per cell line.

ELISAs for cytokine detection

Culture medias from IGR37 and 501mel cells previously treated over time with the SCD inhibitor A939572 (1 uM) were collected, centrifuged at 1,200 rpm, 4°C for 5 min to remove cell debris, and stored at -20 C until use. To quantify cytokine content, specific ELISAs Kits for IL8, IL6 and CXCL1 were used according to the manufacturer´s instructions. Briefly, the samples from different experimental groups, together with Standard samples of known concentrations supplied with the kit, were added to the kit plate, incubated with the kit reagents and analyzed by measuring absorbance at 450 nm. Later, using the Standard samples, a Standard curve was created in GraphPad Prism 7 software to interpolate the sample absorbance values and obtain the Cytokine concentration in each case. Samples from 5 to 10 different experiments were analyzed.

Intracellular cytokines staining for Flow Cytometry

IGR37 and 501mel cells at 60%–70% of confluency were treated with the SCD inhibitor A939572 (1 μM) during 72 h. Within this period the cells were incubated for 12 h in the presence of the protein transport inhibitors Brefeldin A (1000x) and Monensin (1000x). Then, cells were washed with PBS, trypsinized, collected in 1.5 ml tubes and spin down at 1200 rpm for 3 min. Cells were fixed by adding 150 ml IC Fixation Buffer, incubated 15 min at room temperature. Cell permeabilization was performed by adding 1 ml of permeabilization/wash buffer (for 250 ml: 5 ml 10% Saponin, 2.5 ml FBS, 1.25 g BSA, 2.5 ml 10% Azide, and PBS to complete volume). For the antibody staining the conjugated antibody was diluted in permeabilization/wash buffer (1:100) and added to the cells during 1 h at room temperature, protected from light. After the incubation the antibody was removed, the cells were washed twice with permeabilization/wash buffer and finally resuspended in 250 ml of PBS. Flow Cytometry analysis was performed by FACS on a BD FACSCanto II (BD Biosciences), and data were analyzed using FlowJo software (7.6.1).

B16-F1 *in vivo* model

$2x10^5$ B16F1 melanoma cells were subcutaneously administrated into C57BL/6 mice. 13 days after B16 injection, when the tumors reached a size of 3-5 mm in diameter, the mice were divided in two groups: control (n=4) and treated (n=6). Thus, tumor-bearing mice received 25 mg/kg A939572 or vehicle intraperitoneal in 200 μl PBS + 5 % DMSO + 10 % Cremophor (10 μl DMSO, 20 μl Cremophor, 170 μl PBS) twice a day for 5 consecutive days. Then the tumours were collected and processed to perform RNA-seq analysis. All animal experiments were approved by the local government authorities (LANUV, NRW, Germany) and performed according to the institutional and national guidelines for the care and use of laboratory animals.

SW1 cells *in vivo* model

1×10^6 SW1 melanoma cells were injected subcutaneously into the C3H/HeJ mice and the primary tumors were allowed to expand during 1 week. Then animals were divided into 3 different groups, including 10 animals per group: control treated with intraperitoneal vehicle (200 μl PBS + 5 % DMSO + 10 % Cremophor) (Group1); mice treated with intraperitoneal A939572 (25 mg/kg; 200 μl PBS + 5 % DMSO + 10 % Cremophor) for 9 days, twice per day followed by a drug holiday until day 20 (Group 2); and mice treated with A939572 (25 mg/kg; 200 μl PBS + 5 % DMSO + 10 % Cremophor) 1 week after cell inoculation for 16 days, twice per day (Group 3) (Figure 7D). Tumor size was measured twice a week for calculation of tumor volume. At day 20 animals were sacrificed and tumors and lungs were harvested for subsequent analysis. All experimental animal procedures were approved by the Institutional Animal Care and Use Committee of Sanford Burnham Prebys Medical Discovery Institute (approval # 13–130, 16–028, and 17–001) and complied with all relevant ethical regulations for animal testing and research.

Quantification of lung metastasis

Lung metastases were observed 20 days following primary tumor induction. Fixed in 4% para-formaldehyde and paraffin embedded lung tissues were sliced to obtain five serial sections per lung. H&E stain was used to quantify the number and size of metastases under a histology microscope.

HCmel3/adoptive T-cell therapy *in vivo* model:

A previously established mouse model of inflammation-driven resistance to adoptive T-cell therapy (ACT) (Landsberg et al., 2012; Reinhardt et al., 2017) was used to examine SCD expression early and late during therapy. In this model C57BL/6 mice were injected subcutaneously with 4 x 105 HCmel3 cells. Non-treated (NT) mice were killed when tumors reached >10 mm in diameter. Mice were sacrificed between 12 and 20 days after ACT start (early-during-treatment, EDT). Experiments were performed in groups of five and repeated twice. Late relapse (R) melanoma samples and cell lines have been described previously (Landsberg et al., 2012; Reinhardt et al., 2017). ACT with Pmel-1 T cells and microarray gene expression analysis were carried as described previously (Landsberg et al., 2012; Reinhardt et al., 2017). Raw data were previously used (Reinhardt et al., 2017) and are accessible through GEO (GSE40213, GSE71879, GSE99925).

Quantification and statistical analysis

All results are presented as the mean ± standard error of the mean (SEM). The data were analyzed using GraphPad Prism 7 software. Analysis of variance (ANOVA) followed by post hoc Tukey's (for multiple comparisons) test was used in statistical comparisons between more than two groups. Statistical comparisons between two groups were performed using Student t-test. When data were not normally distributed, the nonparametric Kruskal-Wallis or Mann Whitney-U test was applied. The significance level was set at $p \leq 0.05$. All statistical details can be found in the figure legends.

Data availability

The authors declare that all data supporting the findings of this study are available within the article or from the corresponding author upon request. Mass Spectrometry data was deposited at the ProteomeXchange Consortium via the PRIDE partner repository with the dataset identifier PXD009677. RNA-seq Mouse Hcmel12 cells has been deposited at the European Nucleotide Archive dataset identifier PRJEB27878, RNA-seq Mouse B16-F1 cells from mice model has been deposited at the European Nucleotide archive dataset identifier PRJEB33932. All human melanoma cell line RNA-seq data is deposited at GEO accession number GSE137392.

SUPPLEMENTAL INFORMATION

Supplemental Information includes 7 figures, and 6 tables and can be found with this article online.

Supplemental Excel Tables 1-6

Table S1 related to Figure 1A-C

Summary of differential expression from SILAC expt.

Table S2 related to Figure 6A

Triplicate 3'RNA seq analysis showing differential expression in human IGR37 or 501mel after depletion of SCD using siRNA#1 vs control siRNA .

Table S3 related to Figure S5

Triplicate 3'RNA seq analysis showing differential expression in human IGR37 after depletion of SCD for 48 h using siRNA#2 vs control siRNA.

Table S4 related to Figure S5

Triplicate 3'RNA seq analysis showing differential expression in human 501mel cells after depletion of SCD for 48 h using siRNA#2 vs control siRNA

Table S5 related to Figure S5

Triplicate 3'RNA seq analysis showing differential expression in human IGR37 cells after inhibition of SCD for 48 h using A939572 vs DMSO control related to Supplemental Figure 5B

Table S6 related to Figure S6

Triplicate 3'RNA seq analysis showing differential expression in mouse HCmel12 cells after inhibition of SCD using CAY10566 vs DMSO control (Sheet1), and B16 cells after inhibition of SCD using CAY10566 vs DMSO control (Sheet 2) related to Supplemental Figure 6

REFERENCES

Aubert, C., Rouge, F., and Galindo, J.R. (1980). Tumorigenicity of human malignant melanocytes in nude mice in relation to their differentiation in vitro. J Natl Cancer Inst *64*, 1029-1040.

B'Chir, W., Maurin, A.C., Carraro, V., Averous, J., Jousse, C., Muranishi, Y., Parry, L., Stepien, G., Fafournoux, P., and Bruhat, A. (2013). The eIF2alpha/ATF4 pathway is essential for stress-induced autophagy gene expression. Nucleic Acids Res *41*, 7683-7699.

Bald, T., Quast, T., Landsberg, J., Rogava, M., Glodde, N., Lopez-Ramos, D., Kohlmeyer, J., Riesenberg, S., van den Boorn-Konijnenberg, D., Homig-Holzel, C., et al. (2014). Ultraviolet-radiation-induced inflammation promotes angiotropism and metastasis in melanoma. Nature *507*, 109-113.

Bernales, S., McDonald, K.L., and Walter, P. (2006). Autophagy counterbalances endoplasmic reticulum expansion during the unfolded protein response. PLoS biology *4*, e423.

Boyce, M., Bryant, K.F., Jousse, C., Long, K., Harding, H.P., Scheuner, D., Kaufman, R.J., Ma, D., Coen, D.M., Ron, D., et al. (2005). A selective inhibitor of eIF2alpha dephosphorylation protects cells from ER stress. Science *307*, 935-939.

Brabletz, T., Jung, A., Spaderna, S., Hlubek, F., and Kirchner, T. (2005). Opinion: migrating cancer stem cells - an integrated concept of malignant tumour progression. Nat Reviews Cancer *5*, 744-749.

Bunk, B., Kucklick, M., Jonas, R., Munch, R., Schobert, M., Jahn, D., and Hiller, K. (2006). MetaQuant: a tool for the automatic quantification of GC/MS-based metabolome data. Bioinformatics *22*, 2962-2965.

Byun, J.K., Choi, Y.K., Kim, J.H., Jeong, J.Y., Jeon, H.J., Kim, M.K., Hwang, I., Lee, S.Y., Lee, Y.M., Lee, I.K., et al. (2017). A positive feedback loop between sestrin2 and mTORC2 is required for the survival of glutamine-depleted lung cancer cells. Cell Reports *20*, 586-599.

Cai, Y., Crowther, J., Pastor, T., Abbasi Asbagh, L., Baietti, M.F., De Troyer, M., Vazquez, I., Talebi, A., Renzi, F., Dehairs, J., et al. (2016). Loss of Chromosome 8p Governs Tumor Progression and Drug Response by Altering Lipid Metabolism. Cancer Cell *29*, 751-766.

Carracedo, A., Cantley, L.C., and Pandolfi, P.P. (2013). Cancer metabolism: fatty acid oxidation in the limelight. Nat Reviews Cancer *13*, 227-232.

Carreira, S., Goodall, J., Aksan, I., La Rocca, S.A., Galibert, M.D., Denat, L., Larue, L., and Goding, C.R. (2005). Mitf cooperates with Rb1 and activates p21Cip1 expression to regulate cell cycle progression. Nature *433*, 764-769.

Carreira, S., Goodall, J., Denat, L., Rodriguez, M., Nuciforo, P., Hoek, K.S., Testori, A., Larue, L., and Goding, C.R. (2006). Mitf regulation of Dia1 controls melanoma proliferation and invasiveness. Genes Dev *20*, 3426-3439.

Cerami, E., Gao, J., Dogrusoz, U., Gross, B.E., Sumer, S.O., Aksoy, B.A., Jacobsen, A., Byrne, C.J., Heuer, M.L., Larsson, E., et al. (2012). The cBio cancer genomics portal: an open platform for exploring multidimensional cancer genomics data. Cancer Discov *2*, 401-404.

Cheli, Y., Guiliano, S., Botton, T., Rocchi, S., Hofman, V., Hofman, P., Bahadoran, P., Bertolotto, C., and Ballotti, R. (2011). Mitf is the key molecular switch between mouse or human melanoma initiating cells and their differentiated progeny. Oncogene *30*, 2307-2318.

Cheli, Y., Ohanna, M., Ballotti, R., and Bertolotto, C. (2010). Fifteen-year quest for microphthalmia-associated transcription factor target genes. Pigment Cell Melanoma Res *23*, 27-40.

Chung, B., Esmaeili, A.A., Gopalakrishna-Pillai, S., Murad, J.P., Andersen, E.S., Kumar Reddy, N., Srinivasan, G., Armstrong, B., Chu, C., Kim, Y., et al. (2017). Human brain metastatic stroma attracts breast cancer cells via chemokines CXCL16 and CXCL12. NPJ Breast Cancer *3*, 6.

Cox, J., and Mann, M. (2008). MaxQuant enables high peptide identification rates, individualized p.p.b.-range mass accuracies and proteome-wide protein quantification. Nat Biotechnol *26*, 1367-1372.

Currie, E., Schulze, A., Zechner, R., Walther, T.C., and Farese, R.V. (2013). Cellular fatty acid metabolism and cancer. Cell Metab *18*, 153-161.

Damgaard, R.B., Nachbur, U., Yabal, M., Wong, W.W., Fiil, B.K., Kastirr, M., Rieser, E., Rickard, J.A., Bankovacki, A., Peschel, C., et al. (2012). The ubiquitin ligase XIAP recruits LUBAC for NOD2 signaling in inflammation and innate immunity. Mol Cell *46*, 746-758.

Dar, A.A., Majid, S., de Semir, D., Nosrati, M., Bezrookove, V., and Kashani-Sabet, M. (2011). miRNA-205 suppresses melanoma cell proliferation and induces senescence via regulation of E2F1 protein. J Biol Chem *286*, 16606-16614.

Davis, S., Charles, P.D., He, L., Mowlds, P., Kessler, B.M., and Fischer, R. (2017). Expanding Proteome Coverage with CHarge Ordered Parallel Ion aNalysis (CHOPIN) Combined with Broad Specificity Proteolysis. J Proteome Res *16*, 1288-1299.

de Hoon, M.J.L., Imoto, S., Nolan, J., and Miyano, S. (2004). Open source clustering software. Bioinformatics *20*, 1453-1454.

Deng, J., Lu, P.D., Zhang, Y., Scheuner, D., Kaufman, R.J., Sonenberg, N., Harding, H.P., and Ron, D. (2004). Translational repression mediates activation of nuclear factor kappa B by phosphorylated translation initiation factor 2. Mol cell Biol *24*, 10161-10168.

Dobin, A., Davis, C.A., Schlesinger, F., Drenkow, J., Zaleski, C., Jha, S., Batut, P., Chaisson, M., and Gingeras, T.R. (2013). STAR: ultrafast universal RNA-seq aligner. Bioinformatics *29*, 15-21.

Du, J., Widlund, H.R., Horstmann, M.A., Ramaswamy, S., Ross, K., Huber, W.E., Nishimura, E.K., Golub, T.R., and Fisher, D.E. (2004). Critical role of CDK2 for melanoma growth linked to its melanocyte-specific transcriptional regulation by MITF. Cancer Cell *6*, 565-576.

Dugo, M., Nicolini, G., Tragni, G., Bersani, I., Tomassetti, A., Colonna, V., Del Vecchio, M., De Braud, F., Canevari, S., Anichini, A., et al. (2015). A melanoma subtype with intrinsic resistance to BRAF inhibition identified by receptor tyrosine kinases gene-driven classification. Oncotarget *6*, 5118-5133.

Falletta, P., Sanchez-del-Campo, L., Chauhan, J., Effern, M., Kenyon, A., Kershaw, C.J., Siddaway, R., Lisle, R., Freter, R., Daniels, M., et al. (2017). Translation reprogramming is an evolutionarily conserved driver of phenotypic plasticity and therapeutic resistance in melanoma. Genes Dev *31*, 18-33.

Ferguson, J., Smith, M., Zudaire, I., Wellbrock, C., and Arozarena, I. (2017). Glucose availability controls ATF4-mediated MITF suppression to drive melanoma cell growth. Oncotarget *8*, 32946-32959.

Ferreiro, D.U., and Komives, E.A. (2010). Molecular mechanisms of system control of NF-kappaB signaling by IkappaBalpha. Biochemistry *49*, 1560-1567.

Fogh, J., Fogh, J.M., and Orfeo, T. (1977). One hundred and twenty-seven cultured human tumor cell lines producing tumors in nude mice. J Natl Cancer Inst *59*, 221-226.

Fritz, V., Benfodda, Z., Rodier, G., Henriquet, C., Iborra, F., Avances, C., Allory, Y., de la Taille, A., Culine, S., Blancou, H., et al. (2010). Abrogation of de novo lipogenesis by stearoyl-CoA desaturase 1 inhibition interferes with oncogenic signaling and blocks prostate cancer progression in mice. Mol Cancer Ther *9*, 1740-1754.

Gao, J., Aksoy, B.A., Dogrusoz, U., Dresdner, G., Gross, B., Sumer, S.O., Sun, Y., Jacobsen, A., Sinha, R., Larsson, E., et al. (2013). Integrative analysis of complex cancer genomics and clinical profiles using the cBioPortal. Science Signaling *6*, pl1.

García-Jimenéz, C., and Goding, C.R. (2019). Starvation and Pseudo-Starvation as Drivers of Cancer Metastasis through Translation Reprogramming. Cell Metab *29*, 258-267.

Gargalovic, P.S., Imura, M., Zhang, B., Gharavi, N.M., Clark, M.J., Pagnon, J., Yang, W.P., He, A., Truong, A., Patel, S., et al. (2006). Identification of inflammatory gene modules based on variations of human endothelial cell responses to oxidized lipids. Proc Natl Acad Sci USA *103*, 12741-12746.

Garraway, L.A., Widlund, H.R., Rubin, M.A., Getz, G., Berger, A.J., Ramaswamy, S., Beroukhim, R., Milner, D.A., Granter, S.R., Du, J., et al. (2005). Integrative genomic analyses identify MITF as a lineage survival oncogene amplified in malignant melanoma. Nature *436*, 117-122.

Ghanem, G.E., Comunale, G., Libert, A., Vercammen-Grandjean, A., and Lejeune, F.J. (1988). Evidence for alpha-melanocyte-stimulating hormone (alpha-MSH) receptors on human malignant melanoma cells. Int J Cancer *41*, 248-255.

Ghosh, R., Nadiminty, N., Fitzpatrick, J.E., Alworth, W.L., Slaga, T.J., and Kumar, A.P. (2005). Eugenol causes melanoma growth suppression through inhibition of E2F1 transcriptional activity. J Biol Chem *280*, 5812-5819.

Giard, D.J., Aaronson, S.A., Todaro, G.J., Arnstein, P., Kersey, J.H., Dosik, H., and Parks, W.P. (1973). In vitro cultivation of human tumors: establishment of cell lines derived from a series of solid tumors. J Natl Cancer Inst *51*, 1417-1423.

Goding, C.R., and Arnheiter, H. (2019). MITF - The first 25 years. Genes Dev. *33*, 983-1007.

Goodall, J., Carreira, S., Denat, L., Kobi, D., Davidson, I., Nuciforo, P., Sturm, R.A., Larue, L., and Goding, C.R. (2008). Brn-2 represses microphthalmia-associated transcription factor expression and marks a distinct subpopulation of microphthalmia-associated transcription factor-negative melanoma cells. Cancer Res *68*, 7788-7794.

Halaban, R., Cheng, E., Smicun, Y., and Germino, J. (2000). Deregulated E2F transcriptional activity in autonomously growing melanoma cells. J Exp Med *191*, 1005-1016.

Hall, A., Meyle, K.D., Lange, M.K., Klima, M., Sanderhoff, M., Dahl, C., Abildgaard, C., Thorup, K., Moghimi, S.M., Jensen, P.B., et al. (2013). Dysfunctional oxidative phosphorylation makes malignant melanoma cells addicted to glycolysis driven by the (V600E)BRAF oncogene. Oncotarget *4*, 584-599.

Hao, Q., Hansen, J.B., Petersen, R.K., Hallenborg, P., Jorgensen, C., Cinti, S., Larsen, P.J., Steffensen, K.R., Wang, H., Collins, S., et al. (2010). ADD1/SREBP1c activates the PGC1-alpha promoter in brown adipocytes. Biochim Biophys Acta *1801*, 421-429.

Haq, R., Shoag, J., Andreu-Perez, P., Yokoyama, S., Edelman, H., Rowe, G.C., Frederick, D.T., Hurley, A.D., Nellore, A., Kung, A.L., et al. (2013). Oncogenic BRAF regulates oxidative metabolism via PGC1alpha and MITF. Cancer Cell *23*, 302-315.

Harding, H.P., Novoa, I., Zhang, Y., Zeng, H., Wek, R., Schapira, M., and Ron, D. (2000). Regulated translation initiation controls stress-induced gene expression in mammalian cells. Mol Cell *6*, 1099-1108.

Herlyn, M., Thurin, J., Balaban, G., Bennicelli, J.L., Herlyn, D., Elder, D.E., Bondi, E., Guerry, D., Nowell, P., Clark, W.H., et al. (1985). Characteristics of cultured human melanocytes isolated from different stages of tumor progression. Cancer Res *45*, 5670-5676.

Hodgkinson, C.A., Moore, K.J., Nakayama, A., Steingrimsson, E., Copeland, N.G., Jenkins, N.A., and Arnheiter, H. (1993). Mutations at the mouse *microphthalmia* locus are associated with defects in a gene encoding a novel basic-helix-loop-helix-zipper protein. Cell *74*, 395-404.

Hoek, K., and Goding, C.R. (2010). Cancer stem cells versus phenotype switching in melanoma. Pigment Cell Melanoma Res. *23*, 746-759.

Huang, H., Jing, G., Wang, J.J., Sheibani, N., and Zhang, S.X. (2015). ATF4 is a novel regulator of MCP-1 in microvascular endothelial cells. J Inflamm *12*, 31. doi: 10.1186/s12950-015-0076-1.

Igal, R.A. (2016). Stearoyl CoA desaturase-1: New insights into a central regulator of cancer metabolism. Biochim Biophys Acta *1861*, 1865-1880.

Iwamoto, H., Abe, M., Yang, Y., Cui, D., Seki, T., Nakamura, M., Hosaka, K., Lim, S., Wu, J., He, X., et al. (2018). Cancer Lipid Metabolism Confers Antiangiogenic Drug Resistance. Cell Metab *28*, 104-117.

Janikiewicz, J., Hanzelka, K., Dziewulska, A., Kozinski, K., Dobrzyn, P., Bernas, T., and Dobrzyn, A. (2015). Inhibition of SCD1 impairs palmitate-derived autophagy at the step of autophagosome-lysosome fusion in pancreatic beta-cells. J Lipid Res *56*, 1901-1911.

Jose, C., Bellance, N., and Rossignol, R. (2011). Choosing between glycolysis and oxidative phosphorylation: A tumor's dilemma. Biochem Biophys Acta *1807*, 5520561.

Kamphorst, J.J., Cross, J.R., Fan, J., de Stanchina, E., Mathew, R., White, E.P., Thompson, C.B., and Rabinowitz, J.D. (2013). Hypoxic and Ras-transformed cells support growth by scavenging unsaturated fatty acids from lysophospholipids. Proc Natl Acad Sci USA *110*, 8882-8887.

Kim, J.S., Ro, S.H., Kim, M., Park, H.W., Semple, I.A., Park, H., Cho, U.S., Wang, W., Guan, K.L., Karin, M., et al. (2015). Sestrin2 inhibits mTORC1 through modulation of GATOR complexes. Scientific Reports *5*, 9502.

Kim, Y.C., Gomez, F.E., Fox, B.G., and Ntambi, J.M. (2000). Differential regulation of the stearoyl-CoA desaturase genes by thiazolidinediones in 3T3-L1 adipocytes. J Lipid Res *41*, 1310-1316.

Koeberle, A., Loser, K., and Thurmer, M. (2016). Stearoyl-CoA desaturase-1 and adaptive stress signaling. Biochem Biophys Acta *1861*, 1719-1726.

Konieczkowski, D.J., Johannessen, C.M., Abudayyeh, O., Kim, J.W., Cooper, Z.A., Piris, A., Frederick, D.T., Barzily-Rokni, M., Straussman, R., Haq, R., et al. (2014). A melanoma cell state distinction influences sensitivity to MAPK pathway inhibitors. Cancer Discov *4*, 816-827.

Landsberg, J., Kohlmeyer, J., Renn, M., Bald, T., Rogava, M., Cron, M., Fatho, M., Lennerz, V., Wolfel, T., Holzel, M., et al. (2012). Melanomas resist T-cell therapy through inflammation-induced reversible dedifferentiation. Nature *490*, 412-416.

Li, J., Condello, S., Thomes-Pepin, J., Ma, X., Xia, Y., Hurley, T.D., Matei, D., and Cheng, J.X. (2017). Lipid desaturation is a metabolic marker and therapeutic target of ovarian cancer stem cells. Cell Stem Cell *20*, 303-314 e305.

Li, X., Qi, Y., Ma, X., Huang, F., Guo, H., Jiang, X., Hong, J., Lin, D., Cui, B., Ning, G., et al. (2013). Chemokine (C-C motif) ligand 20, a potential biomarker for Graves' disease, is regulated by osteopontin. PloS one *8*, e64277.

Lin, J.H., Li, H., Yasumura, D., Cohen, H.R., Zhang, C., Panning, B., Shokat, K.M., Lavail, M.M., and Walter, P. (2007). IRE1 signaling affects cell fate during the unfolded protein response. Science *318*, 944-949.

Louphrasitthiphol, P., Ledaki, I., Chauhan, J., Falletta, P., Siddaway, R., Buffa, F.M., Mole, D.R., Soga, T., and Goding, C.R. (2019). MITF controls the TCA cycle to modulate the melanoma hypoxia response. Pigment Cell Melanoma Research. *32*, 792-808.

Magnúsdóttir, E., Dietmann, S., Murakami, K., Günesdogan, U., Tang, F., Bao, S., Diamanti, E., Lao, K., Gottgens, B., and Azim Surani, M. (2013). A tripartite transcription factor network regulates primordial germ cell specification in mice. Nat Cell Biology *15*, 905-915.

Marchiq, I., and Pouyssegur, J. (2016). Hypoxia, cancer metabolism and the therapeutic benefit of targeting lactate/H(+) symporters. J Mol Med *94*, 155-171.

Martin, M. (2011). Cutadapt Removes Adapter Sequences From High-Throughput Sequencing Reads. EMBnet J. *17*, 10-12

Marusyk, A., and Polyak, K. (2010). Tumor heterogeneity: causes and consequences. Biochim Biophys Acta *1805*, 105-117.

Mason, P., Liang, B., Li, L., Fremgen, T., Murphy, E., Quinn, A., Madden, S.L., Biemann, H.P., Wang, B., Cohen, A., et al. (2012). SCD1 inhibition causes cancer cell death by depleting mono-unsaturated fatty acids. PloS one *7*, e33823.

Mlecnik, B., Bindea, G., Kirilovsky, A., Angell, H.K., Obenauf, A.C., Tosolini, M., Church, S.E., Maby, P., Vasaturo, A., Angelova, M., et al. (2016). The tumor microenvironment and Immunoscore are critical determinants of dissemination to distant metastasis. Sci Transl Med *8*, 327ra326.

Muller, J., Krijgsman, O., Tsoi, J., Robert, L., Hugo, W., Song, C., Kong, X., Possik, P.A., Cornelissen-Steijger, P.D., Foppen, M.H., et al. (2014). Low MITF/AXL ratio predicts early resistance to multiple targeted drugs in melanoma. Nat Commun *5*, 5712.

Nieto, M.A., Huang, R.Y., Jackson, R.A., and Thiery, J.P. (2016). EMT: 2016. Cell *166*, 21-45.

Ogasawara, Y., Itakura, E., Kono, N., and Mizushima, N. (2014). Stearoyl-CoA desaturase 1 activity is required for autophagosome formation. J. Biol.Chem. *289*, 23938-23950.

Pandolfi, S., Montagnani, V., Lapucci, A., and Stecca, B. (2015). HEDGEHOG/GLI-E2F1 axis modulates iASPP expression and function and regulates melanoma cell growth. Cell Death Differ *22*, 2006-2019.

Parmenter, T.J., Kleinschmidt, M., Kinross, K.M., Bond, S.T., Li, J., Kaadige, M.R., Rao, A., Sheppard, K.E., Hugo, W., Pupo, G.M., et al. (2014). Response of BRAF-mutant melanoma to BRAF inhibition is mediated by a network of transcriptional regulators of glycolysis. Cancer Discov *4*, 423-433.

Pascual, G., Avgustinova, A., Mejetta, S., Martín, M., Castellanos, A., Attolini, C.S.-O., Berenguer, A., Prats, N., Toll, A., Hueto, J.A., et al. (2016). Targeting metastasis-initiating cells through the fatty acid receptor CD36. Nature *541*, 41-45.

Peck, B., Schug, Z.T., Zhang, Q., Dankworth, B., Jones, D.T., Smethurst, E., Patel, R., Mason, S., Jiang, M., Saunders, R., et al. (2016). Inhibition of fatty acid desaturation is detrimental to cancer cell survival in metabolically compromised environments. Cancer & Metab *4*, 6. doi: 10.1186/s40170-016-0146-8

Pinkham, K., Park, D.J., Hashemiaghdam, A., Kirov, A.B., Adam, I., Rosiak, K., da Hora, C.C., Teng, J., Cheah, P.S., Carvalho, L., et al. (2019). Stearoyl CoA Desaturase Is Essential for Regulation of endoplasmic reticulum homeostasis and tumor growth in glioblastoma cancer stem cells. Stem Cell Reports *12*, 712-727.

Pisanu, M.E., Maugeri-Sacca, M., Fattore, L., Bruschini, S., De Vitis, C., Tabbi, E., Bellei, B., Migliano, E., Kovacs, D., Camera, E., et al. (2018). Inhibition of Stearoyl-CoA desaturase 1 reverts BRAF and MEK inhibition-induced selection of cancer stem cells in BRAF-mutated melanoma. J Exp Clin Cancer Res *37*, 318.

Presler, M., Wojtczyk-Miaskowska, A., Schlichtholz, B., Kaluzny, A., Matuszewski, M., Mika, A., Sledzinski, T., and Swierczynski, J. (2018). Increased expression of the gene encoding stearoyl-CoA desaturase 1 in human bladder cancer. Mol Cell Biochem. *447*, 217-224.

Quail, D.F., and Joyce, J.A. (2013). Microenvironmental regulation of tumor progression and metastasis. Nat Med *19*, 1423-1437.

Rambow, F., Rogiers, A., Marin-Bejar, O., Aibar, S., Femel, J., Dewaela, M., Karras, P., Brown, D., Chang, Y.H., Debiec-Rychter, M., et al. (2018). Towards minimal residual disease-directed therapy in melanoma. Cell *174*, 843-855.

Rambow, F., Marine, J.C., and Goding, C.R. (2019). Melanoma plasticity and phenotypic diversity: therapeutic barriers and opportunities Genes Dev *33*, 1295-1318.

Reinhardt, J., Landsberg, J., Schmid-Burgk, J.L., Ramis, B.B., Bald, T., Glodde, N., Lopez-Ramos, D., Young, A., Ngiow, S.F., Nettersheim, D., et al. (2017). MAPK Signaling and Inflammation Link Melanoma Phenotype Switching to Induction of CD73 during Immunotherapy. Cancer Res *77*, 4697-4709.

Riesenberg, S., Groetchen, A., Siddaway, R., Bald, T., Reinhardt, J., Smorra, D., Kohlmeyer, J., Renn, M., Phung, B., Aymans, P., et al. (2015). MITF and c-Jun antagonism interconnects melanoma dedifferentiation with pro-inflammatory cytokine responsiveness and myeloid cell recruitment. Nat Commun *6*, 8755 DOI:8710.1038 ncomss9755.

Riverso, M., Montagnani, V., and Stecca, B. (2017). KLF4 is regulated by RAS/RAF/MEK/ERK signaling through E2F1 and promotes melanoma cell growth. Oncogene *36*, 3322-3333.

Robinson, M.D., McCarthy, D.J., and Smyth, G.K. (2010). edgeR: a Bioconductor package for differential expression analysis of digital gene expression data. Bioinformatics *26*, 139-140.

Roesch, A., Vultur, A., Bogeski, I., Wang, H., Zimmermann, K.M., Speicher, D., Korbel, C., Laschke, M.W., Gimotty, P.A., Philipp, S.E., et al. (2013). Overcoming intrinsic multidrug resistance in melanoma by blocking the mitochondrial respiratory chain of slow-cycling JARID1B(high) cells. Cancer Cell *23*, 811-825.

Rouaud, F., Hamouda-Tekaya, N., Cerezo, M., Abbe, P., Zangari, J., Hofman, V., Ohanna, M., Mograbi, B., El-Hachem, N., Benfodda, Z., et al. (2018). E2F1 inhibition mediates cell death of metastatic melanoma. Cell Death Disease *9*, 527.

Rysman, E., Brusselmans, K., Scheys, K., Timmermans, L., Derua, R., Munck, S., Van Veldhoven, P.P., Waltregny, D., Daniels, V.W., Machiels, J., et al. (2010). De novo lipogenesis protects cancer cells from free radicals and chemotherapeutics by promoting membrane lipid saturation. Cancer Res *70*, 8117-8126.

Rzymski, T., Milani, M., Singleton, D.C., and Harris, A.L. (2009). Role of ATF4 in regulation of autophagy and resistance to drugs and hypoxia. Cell Cycle *8*, 3838-3847.

Saez-Ayala, M., Montenegro, M.F., Sanchez-Del-Campo, L., Fernandez-Perez, M.P., Chazarra, S., Freter, R., Middleton, M., Pinero-Madrona, A., Cabezas-Herrera, J., Goding, C.R., et al. (2013). Directed phenotype switching as an effective antimelanoma strategy. Cancer Cell *24*, 105-119.

Saldanha, A.J. (2004). Java Treeview--extensible visualization of microarray data. Bioinformatics *20*, 3246-3248.

Schroeder, F., and Gardiner, J.M. (1984). Membrane lipids and enzymes of cultured high- and low-metastatic B16 melanoma variants. Cancer Research *44*, 3262-3269.

Shao, W., and Espenshade, P.J. (2012). Expanding roles for SREBP in metabolism. Cell Metab *16*, 414-419.

Srivastava, S.P., Kumar, K.U., and Kaufman, R.J. (1998). Phosphorylation of eukaryotic translation initiation factor 2 mediates apoptosis in response to activation of the double-stranded RNA-dependent protein kinase. J Biol Chem *273*, 2416-2423.

Strub, T., Kobi, D., Kulodrovic, D., and Davidson, I. (2011). A POU3F2-MITF-SHC4 axis in phenotype switching of melanoma cells. In A POU3F2-MITF-SHC4 axis in phenotype switching of melanoma cells. M. Murph, ed. (InTech).

Subramanian, A., Tamayo, P., Mootha, V.K., Mukherjee, S., Ebert, B.L., Gillette, M.A., Paulovich, A., Pomeroy, S.L., Golub, T.R., Lander, E.S., et al. (2005). Gene set enrichment analysis: a knowledge-based approach for interpreting genome-wide expression profiles. Proc Natl Acad Sci USA *102*, 15545-15550.

Tabor, D.E., Kim, J.B., Spiegelman, B.M., and Edwards, P.A. (1999). Identification of conserved cis-elements and transcription factors required for sterol-regulated transcription of stearoyl-CoA desaturase 1 and 2. J Biol Chem *274*, 20603-20610.

Tam, A.B., Mercado, E.L., Hoffmann, A., and Niwa, M. (2012). ER stress activates NF-kappaB by integrating functions of basal IKK activity, IRE1 and PERK. PloS one *7*, e45078.

Tyanova, S., Temu, T., Sinitcyn, P., Carlson, A., Hein, M.Y., Geiger, T., Mann, M., and Cox, J. (2016). The Perseus computational platform for comprehensive analysis of (prote)omics data. Nat Methods *13*, 731-740.

Vazquez, F., Lim, J.H., Chim, H., Bhalla, K., Girnun, G., Pierce, K., Clish, C.B., Granter, S.R., Widlund, H.R., Spiegelman, B.M., et al. (2013). PGC1alpha expression defines a subset of human melanoma tumors with increased mitochondrial capacity and resistance to oxidative stress. Cancer Cell *23*, 287-301.

Ventura, R., Mordec, K., Waszczuk, J., Wang, Z., Lai, J., Fridlib, M., Buckley, D., Kemble, G., and Heuer, T.S. (2015). Inhibition of de novo Palmitate Synthesis by Fatty Acid Synthase Induces Apoptosis in Tumor Cells by Remodeling Cell Membranes, Inhibiting Signaling Pathways, and Reprogramming Gene Expression. EBioMedicine *2*, 808-824.

Verfaillie, A., Imrichova, H., Atak, Z.K., Dewaele, M., Rambow, F., Hulselmans, G., Christiaens, V., Svetlichnyy, D., Luciani, F., Van den Mooter, L., et al. (2015). Decoding the regulatory landscape of melanoma reveals TEADS as regulators of the invasive cell state. Nat Commun *6*, 6683.

Vizcaino, J.A., Csordas, A., del-Toro, N., Dianes, J.A., Griss, J., Lavidas, I., Mayer, G., Perez-Riverol, Y., Reisinger, F., Ternent, T., et al. (2016). 2016 update of the PRIDE database and its related tools. Nucleic Acisds Res *44*, D447-456.

Volmer, R., and Ron, D. (2015). Lipid-dependent regulation of the unfolded protein response. Curr Op Cell Biol *33*, 67-73.

Volmer, R., van der Ploeg, K., and Ron, D. (2013). Membrane lipid saturation activates endoplasmic reticulum unfolded protein response transducers through their transmembrane domains. Proc Natl Acad Sci USA *110*, 4628-4633.

von Roemeling, C.A., Marlow, L.A., Wei, J.J., Cooper, S.J., Caulfield, T.R., Wu, K., Tan, W.W., Tun, H.W., and Copland, J.A. (2013). Stearoyl-CoA desaturase 1 is a novel molecular therapeutic target for clear cell renal cell carcinoma. Clin Cancer Res *19*, 2368-2380.

Vriens, K., Christen, S., Parik, S., Broekaert, D., Yoshinaga, K., Talebi, A., Dehairs, J., Escalona-Noguero, C., Schmieder, R., Cornfield, T., et al. (2019). Evidence for an alternative fatty acid desaturation pathway increasing cancer plasticity. Nature *566*, 403-406.

Williams, K.J., Argus, J.P., Zhu, Y., Wilks, M.Q., Marbois, B.N., York, A.G., Kidani, Y., Pourzia, A.L., Akhavan, D., Lisiero, D.N., et al. (2013). An essential requirement for the SCAP/SREBP signaling axis to protect cancer cells from lipotoxicity. Cancer Res *73*, 2850-2862.

Wolfson, R.L., Chantranupong, L., Saxton, R.A., Shen, K., Scaria, S.M., Cantor, J.R., and Sabatini, D.M. (2016). Sestrin2 is a leucine sensor for the mTORC1 pathway. Science *351*, 43-48.

Xie, H., Tang, C.H., Song, J.H., Mancuso, A., Del Valle, J.R., Cao, J., Xiang, Y., Dang, C.V., Lan, R., Sanchez, D.J., et al. (2018). IRE1alpha RNase-dependent lipid homeostasis promotes survival in Myc-transformed cancers. J Clin Invest *128*, 1300-1316.

Ye, J., Palm, W., Peng, M., King, B., Lindsten, T., Li, M.O., Koumenis, C., and Thompson, C.B. (2015). GCN2 sustains mTORC1 suppression upon amino acid deprivation by inducing Sestrin2. Genes Dev *29*, 2331-2336.

Zaidi, N., Royaux, I., Swinnen, J.V., and Smans, K. (2012). ATP citrate lyase knockdown induces growth arrest and apoptosis through different cell- and environment-dependent mechanisms. Mol Cancer Ther *11*, 1925-1935.

Zakut, R., Perlis, R., Eliyahu, S., Yarden, Y., Givol, D., Lyman, S.D., and Halaban, R. (1993). KIT ligand (mast cell growth factor) inhibits the growth of KIT- expressing melanoma cells. Oncogene *8*, 2221-2229.

Zhang, C., Bai, N., Chang, A., Zhang, Z., Yin, J., Shen, W., Tian, Y., Xiang, R., and Liu, C. (2013). ATF4 is directly recruited by TLR4 signaling and positively regulates TLR4-trigged cytokine production in human monocytes. Cell Mol Immunol *10*, 84-94.

Zhang, G., Frederick, D.T., Wu, L., Wei, Z., Krepler, C., Srinivasan, S., Chae, Y.C., Xu, X., Choi, H., Dimwamwa, E., et al. (2016). Targeting mitochondrial biogenesis to overcome drug resistance to MAPK inhibitors. J Clin Invest *125*, 1834-1856.

Zhang, M., Di Martino, J.S., Bowman, R.L., Campbell, N.R., Baksh, S.C., Simon-Vermot, T., Kim, I.S., Haldeman, P., Mondal, C., Yong-Gonzales, V., et al. (2018). Adipocyte-Derived Lipids Mediate Melanoma Progression via FATP Proteins. Cancer Discov *8*, 1006-1025.

KEY RESOURCES TABLE

REAGENT or RESOURCE	SOURCE	IDENTIFIER
Antibodies		
Rabbit monoclonal anti-ATF4 (D4B8)	Cell Signaling	Cat# 11815
Mouse monoclonal anti-MITF (C5)	Abcam	Cat# ab12039
Mouse monoclonal anti-GAPDH (6C5)	Santa Cruz Biotechnologies	Cat# sc-32233
Mouse monoclonal anti-SCD1[CD.E10]	Abcam	Cat# ab19862
Rabbit polyclonal anti-SCD	Atlas Antibodies	Cat# HPA012107
Mouse monoclonal anti-FLAG® M2 affinity isolated	Sigma Aldrich	Cat# F1804
Rabbit polyclonal anti-alpha Tubulin	Abcam	Cat# ab18251
Mouse polyclonal anti- ERK 2 (D-2)	Santa Cruz Biotechnologies	Cat# sc-1647
Rabbit polyclonal anti-ACLY [EP704Y]	Abcam	Cat# ab40793
Rabbit monoclonal anti-CPT1a	Cell Signaling	Cat# 12252
Rabbit monoclonal anti-AXL (C89E7)	Cell Signaling	Cat# 8661
Rabbit polyclonal anti-LC3B	Cell Signaling	Cat# 2775
Mouse monoclonal anti-Fibronectin 1	BD	Cat# 610078
Rabbit polyclonal anti-IκBα	Cell Signaling	Cat# 9242
Rabbit monoclonal anti-Brn2/POU3F2 (D2C1L)	Cell Signaling	Cat#12137
Rabbit monoclonal anti-PARP (46D11)	Cell Signaling	Cat#9532S
Rabbit polyclonal anti-Cleaved PARP (Asp214) Antibody (Human Specific)	Cell Signaling	Cat#9541
Rabbit polyclonal anti-E2F1	Cell Signaling	Cat#3742S
Rabbit monoclonal anti-BiP (C50B12)	Cell Signaling	Cat#3177
Rabbit monoclonal anti-PERK (C33E10)	Cell Signaling	Cat#3192
Rabbit monoclonal anti-SESTRIN2	Protein Tech	Cat#10795-1-AP
IL-8/APC antibody	BioLegend	Cat#511410
IL-6/APC antibody	BioLegend	Cat#501112
Alexa Fluor 488 donkey anti-mouse IgG (H+L)	Invitrogen	Cat#A21202
Alexa Fluor 488 donkey anti-rabbit IgG (H+L)	Invitrogen	Cat#A21206
Alexa Fluor 546 donkey anti-mouse IgG (H+L)	Invitrogen	Cat#A10036
Alexa Fluor 546 donkey anti-rabbit IgG (H+L)	Invitrogen	Cat#A10040
Bacterial and Virus Strains		
Subcloning Efficiency DH5α bacteria	Invitrogen	Cat#18265-017
Biological Samples		
Chemicals, Peptides, and Recombinant Proteins		
SCD1 inhibitor A939572	BioVision	Cat#1716-1,5
SCD1 inhibitor CAY10566	Cayman Chemical	Cat#10012562
Salubrinal	Calbiochem	Cat#324897-5MG
TNFα	GIBCO	Cat# PHC3016
Doxycycline	Sigma	Cat#D9891-10G
Glutamax DMEM media	GIBCO	Cat#31966021

RPMI 1640 media	GIBCO	Cat#21875-034
MEM media	GIBCO	Cat#21090-022
DMEM media	Lonza	Cat#12-604F
DMEM for SILAC media	Invitrogen	Cat#88364
Dialyzed Fetal Bovine Serum	Biosera	Cat# FB-1001D/500
Normal Fetal Bovine Serum	Sigma	Cat#F4135
Lipid depleted Fetal Bovine Serum	Biowest	Cat#S181L-100
L-Glutamine (200 mM)	GIBCO	Cat#25030-024
L-Serine	Sigma	Cat#S-4311
L-Glycine	Fisher Scientific	Cat# G/0800/60
Heptadecanoic acid	MP Biomedicals	Cat# 05207583
Fatty acid methyl esters-Supelco 37 Component FAME Mix	Sigma	Cat#CRM47885 SUPELCO
Oleic acid	Sigma	Cat#O1383
Palmitoleic acid	Sigma	Cat# P9417
EasyTag™ EXPRESS35S Protein Labeling Mix, [35S]-, 7mCi	Perkin Elmer	Cat#NEG772007 MC
Lipofectamine RNAiMAX	Invitrogen	Cat#13778-150
OptiMem	GIBCO	Cat#31985-062
FuGENE6	Promega	Cat#E2692
BSA	Sigma	Cat#A9647-100G
Bovine Type I Atelo-Collagen Solution, 3 mg/ml, 100 ml	Advanced Biomatrix	Cat#5005-100ML
Hoechst 33258	Life Tech	Cat#H3569
Saponin	Fluka	Cat#47036
IC Fixation Buffer	eBioscience	Cat#00-8222-49
Sodium Azide	Sigma	Cat#S2002
Brefeldin A Solution	BioLegend	Cat#420601
Monensin Solution	BioLegend	Cat#420701
Cremophor	Merck Chemicals Ltd	Cat#238470-1SET
Critical Commercial Assays		
QuantiTect reverse transcription kit	Qiagen	Cat#205313
ECL detection kit	Amersham Biosciences	Cat#GE Healthcare, RPN2106
RNA extraction RNeasy Mini Kit	Qiagen	Cat#74106
Dual-Luciferase reporter Assay System	Promega	Cat#E1960
MycoAlert™ mycoplasma detection kit	Lonza	Cat#LT07-318
Pierce™ BCA Protein Assay Kit	ThermoFisher	Cat#23225
CellEvent Caspase-3/7 Green flow cytometry assay kit	ThermoFisher	Cat#C10427
IL-8 Human Coated ELISA Kit	ThermoFisher	Cat# BMS204/3
IL-6 Human Coated ELISA Kit	ThermoFisher	Cat# BMS213HS
CXCL1-GRO-aplha Human Coated ELISA Kit	ThermoFisher	Cat# BMS2122
Deposited Data		
RNA-seq data for Human melanoma cell lines is available for referees at GEO	GEO	GSE137392

RNA-seq Mouse Hcmel12 cells has been deposited at the European Nucleotide archive	http://www.ebi.ac.uk/ena/data/view/PRJEB27878	PRJEB27878
RNA-seq Mouse B16-F1 cells from mice model has been deposited at the European Nucleotide archive	http://www.ebi.ac.uk/ena/data/view/	PRJEB33932
SILAC data has been uploaded tot the PRIDE repository	http://www.ebi.ac.uk/pride	PXD010254
Experimental Models: Cell Lines		
IGR37 Human melanoma cell line (female)	Obtained from Luisa Lanfrancone	(Aubert et al., 1980)
IGR39 Human melanoma cell line (female)	Obtained from Luisa Lanfrancone	(Aubert et al., 1980)
501mel Human melanoma cell line (female)	Obtained from Ruth Halaban, Yale	(Zakut et al., 1993)
A375M Human melanoma cell line (male)	Obtained from ATCC	(Fogh et al., 1977; Giard et al., 1973)(Fogh et al., 1977; Giard et al., 1973)
SKmel28 Human melanoma cell line (male)	Obtained from ATCC	(Fogh et al., 1977)
SKmel30.1 Human melanoma cell line (female)	Derivative of SKmel30	
HBL Human melanoma cell line (female)	Obtained from Ghanem Lab, Brussels	(Ghanem et al., 1988)
WM852 Human melanoma cell line (female)	Obtained from Meenhard Herlyn	(Herlyn et al., 1985)
HBL-100 Human breast cell line (female)	Obtained from Ghanem Lab, Brussels	
Engineered doxycycline-inducible ATF4 501mel Human melanoma cell line	In house	(Falletta et al., 2017)
Engineered doxycycline-inducible ATF4 SKmel28 Human melanoma cell line	In house	(Falletta et al., 2017)
Engineered doxycycline-inducible ATF4 B16 Mouse melanoma cell line	In house	(Falletta et al., 2017)
Engineered doxycycline-inducible MITF 501mel Human melanoma cell line	In house	(Falletta et al., 2017)
B16F1 mouse melanoma cell line	Obtained from ATCC	ATCC CRL-6323
HCmel12 mouse melanoma cell line	Obtained from Michael Hölzel	(Bald et al., 2014)
HCmel10 mouse melanoma cell line	Michael Hölzel lab	(Riesenberg et al., 2015)
HCmel3 mouse melanoma cell line	Michael Hölzel lab	(Landsberg et al., 2012; Riesenberg et al., 2015)
SW1 mouse melanoma cell line	Ze'ev Ronai lab	
Oligonucleotides		
Human A20 RT qPCR primers F 5´-3´: ATGCACCGATACACACTGGA R 5´-3´: GGATGATCTCCCGAAACTGA	Gift of Prof. Mads Gyrd-Hansen	

Human ACLY RT qPCR primers F 5´-3´: GTC TAT GTC CTT GAC TTG GCG R 5´-3´: ACT TTT GGC ATC GAG GTC TG	Sigma	This study
Human ATF4 RT qPCR primers F 5´-3´: TCA AAC CTC ATG GGT TCT CC R 5´-3´: GTG TCA TCC AAC GTG GTC AG	Sigma	(Falletta et al., 2017)
Human B2mg RT qPCR primers F 5´-3´: TGCTGTCTCCATGTT TGATGTATCT R 5´-3´: TCTCTGCTCCCCACCTCTAAGT	Sigma	This study
Human CCL2 RT qPCR primers F 5´-3´: AGTCTCTGCCGCCCTTCT R 5´-3´: GTGACTGGGGCATTGATTG	Gift from Prof. Mads Gyrd-Hansen	
Human CCL20 RT qPCR primers F 5´-3´: TGCTGTACCAAGAGTTTGCTC R 5´-3´: CGCACACAGACAACTTTTTCTTT	Sigma	(Li et al., 2013)
Human CPT1a RT qPCR primers F 5´-3´: ACCTCCGTAGCTGACTCG R 5´-3´: TGACCGTGAACTGAAAGGC	Sigma	This study
Human CXCL1 RT qPCR primers F 5´-3´: TCCTGCATCCCCCATAGTTA R 5´-3´: CTTCAGGAACAGCCACCAGT	Gift from Prof. Mads Gyrd-Hansen	
Human CXCL16 RT qPCR primers F 5´-3´: GGCCCACCAGAAGCATTTAC R 5´-3´: CTGAAGATGCCCCCTCTGAG	Sigma	(Chung et al., 2017)
Human FASN RT qPCR primers F 5´-3´: CAAGGACACAGTCACCATCTC R 5´-3´: CATGAAGTAGGAGTGGAAGGC	Sigma	This study
Human IL6 RT qPCR primers F 5´-3´: ATTCTGCGCAGCTTTAAGGA R 5´-3´: GAGGTGCCCATGCTACATTT	Gift from Prof. Mads Gyrd-Hansen	
Human IL8 RT qPCR primers F 5´-3´: TCTGGCAACCCTAGTCTGCT R 5´-3´: AAACCAAGGCACAGTGGAAC	Gift from Prof. Mads Gyrd-Hansen	
Human MITF RT qPCR primers F 5´-3´: AGAGCAAAACAGGGCAGAG R 5´-3´: GCAAAGCAGGATCCATCAAG	Sigma	This study
Human PGC1a RT qPCR primers F 5´-3´: GTAAATCTGCGGGATGATGG R 5´-3´: AATTGCTTGCGTCCACAAA	Sigma	(Vazquez et al., 2013)
Human SCD RT qPCR primers F 5´-3´: CTCTGCTACACTTGGGAGCC R 5´-3´: GAGCTCCTGCTGTTATGCCC	Sigma	This study
Human XBP1s RT qPCR primers F 5´-3´: TGCTGAGTCCGCAGCAGGTG R 5´-3´: GCTGGCAGGCTCTGGGGAAG	Sigma	
Human XPP1s RT-PCR primers F 5´-3´: TTACGAGAGAAAACTCATGGC R 5´-3´: GGGTCCAAGTTGTCCAGAATGC	Sigma	(Lin et al., 2007)
Human CHOP primers F 5´-3´:GTTAAAGATGAGCGGGTGGC R 5´-3´:TGCAGTTGGATCAGTCTGCTT	Sigma	This study
Human SESN2 primers F 5´-3´: GAC CATGGC TAC TCG CTG AT R 5´-3´: GCTGCCTGGAACTTCTCATC	Sigma	(Baozhong Zhao et al 2014)
Human RelA (p65-NFκB) F 5´-3´: TAAGCAGAAGCATTAACTTCTCTGGA R 5´-3': CCTGCTTCTGTCTCTAGGAGAGTA		This study
siRNA control	Qiagen	Cat#1027281

siRNA MITF 1 5′-AAAGCAGTACCTTTCTACCAC-3′	Sigma	(Falletta et al., 2017)
siRNA MITF 2 5′-TGGCTATGCTTACGCTTAA-3′	Sigma	This study
SCD siRNA (h), 10 μM (siSCD#1)	Santa Cruz Biotechnologies	sc-36464
SMARTpool: ON-TARGETplus SCD siRNA (siSCD#2)	Dharmacon Inc	L-005061-00-0005
Recombinant DNA		
Plasmid Piggybac expression system		(Magnúsdóttir et al., 2013)
NFκB reporter construct pBIIXluc	Gift from Prof. Mads Gyrd-Hansen	(Damgaard et al., 2012)
Thymidine kinase-renilla luciferase construct	Gift from Prof. Mads Gyrd-Hansen	(Damgaard et al., 2012)
Software and Algorithms		
MetaQuant		(Bunk et al., 2006)
ImageJ	https://imagej.nih.gov/ij/	
Cutadapt		(Martin, 2011)
CGDS-R		(Cerami et al., 2012; Gao et al., 2013)
STAR		(Dobin et al., 2013)
EdgeR		(Robinson et al., 2010)
Gene Cluster 3.0		(de Hoon et al., 2004)
TreeView		(Saldanha, 2004)
javaGSEA2-3.0		(Subramanian et al., 2005)
GraphPad Prism 7		https://www.graphpad.com
Perseus		(Tyanova et al., 2016)
Other		
TCGA analysis R-script		(Riesenberg et al., 2015)

Figure 1

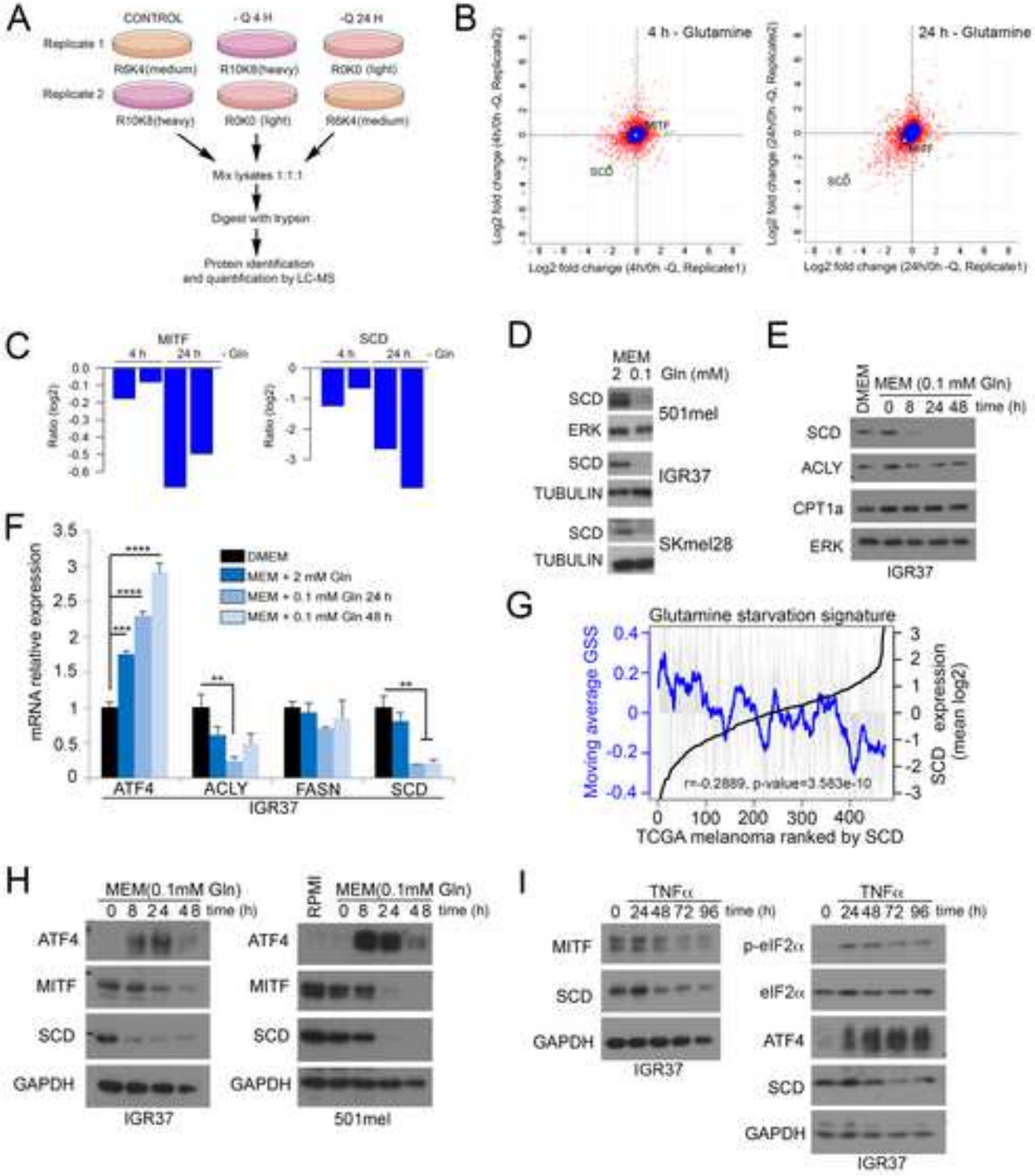

Figure 1

Figure 2

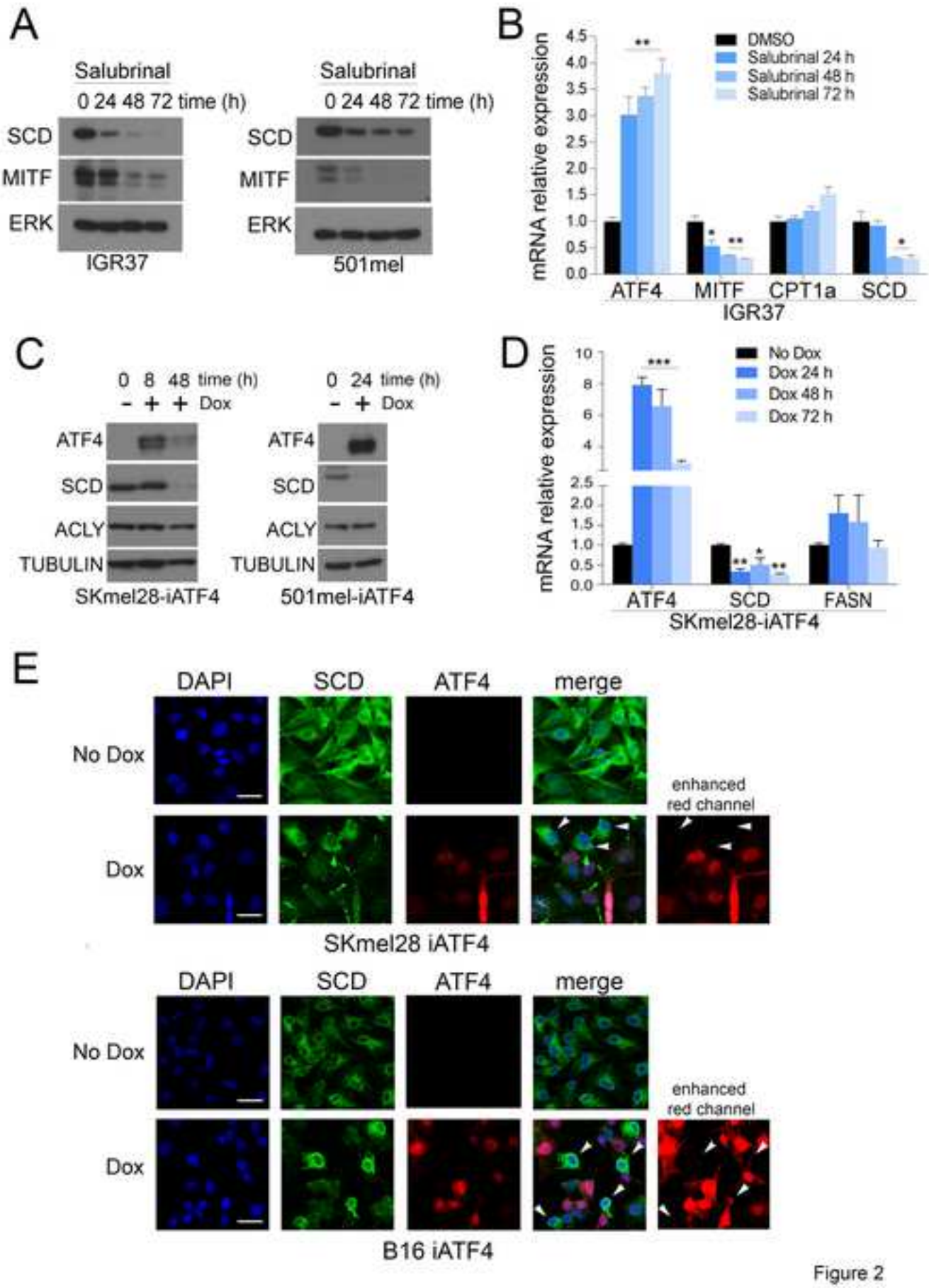

Figure 2

Figure 3

Click here to access/download;Figure;FIGURE 3SR.tif

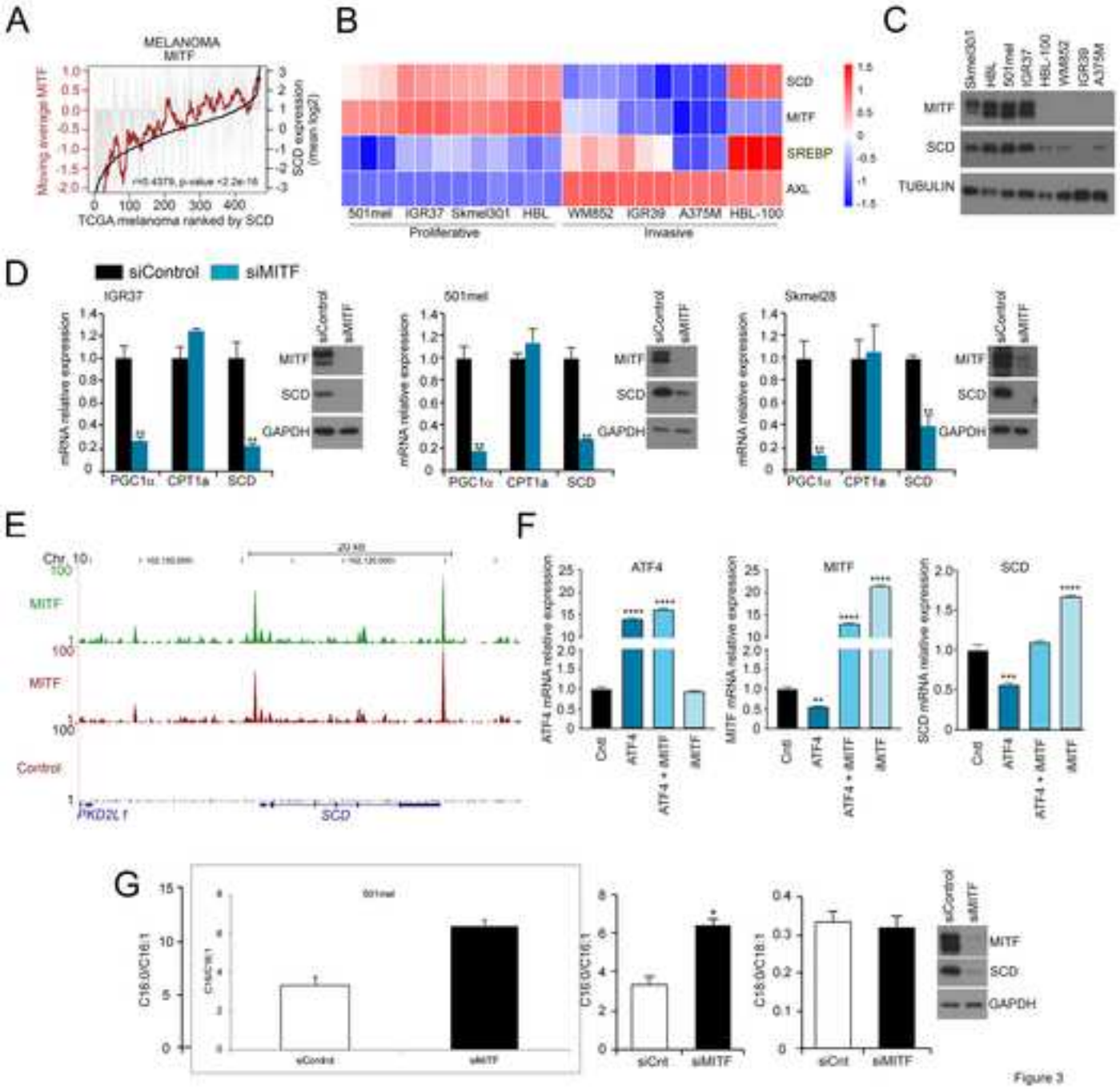

Figure 3

Figure 4

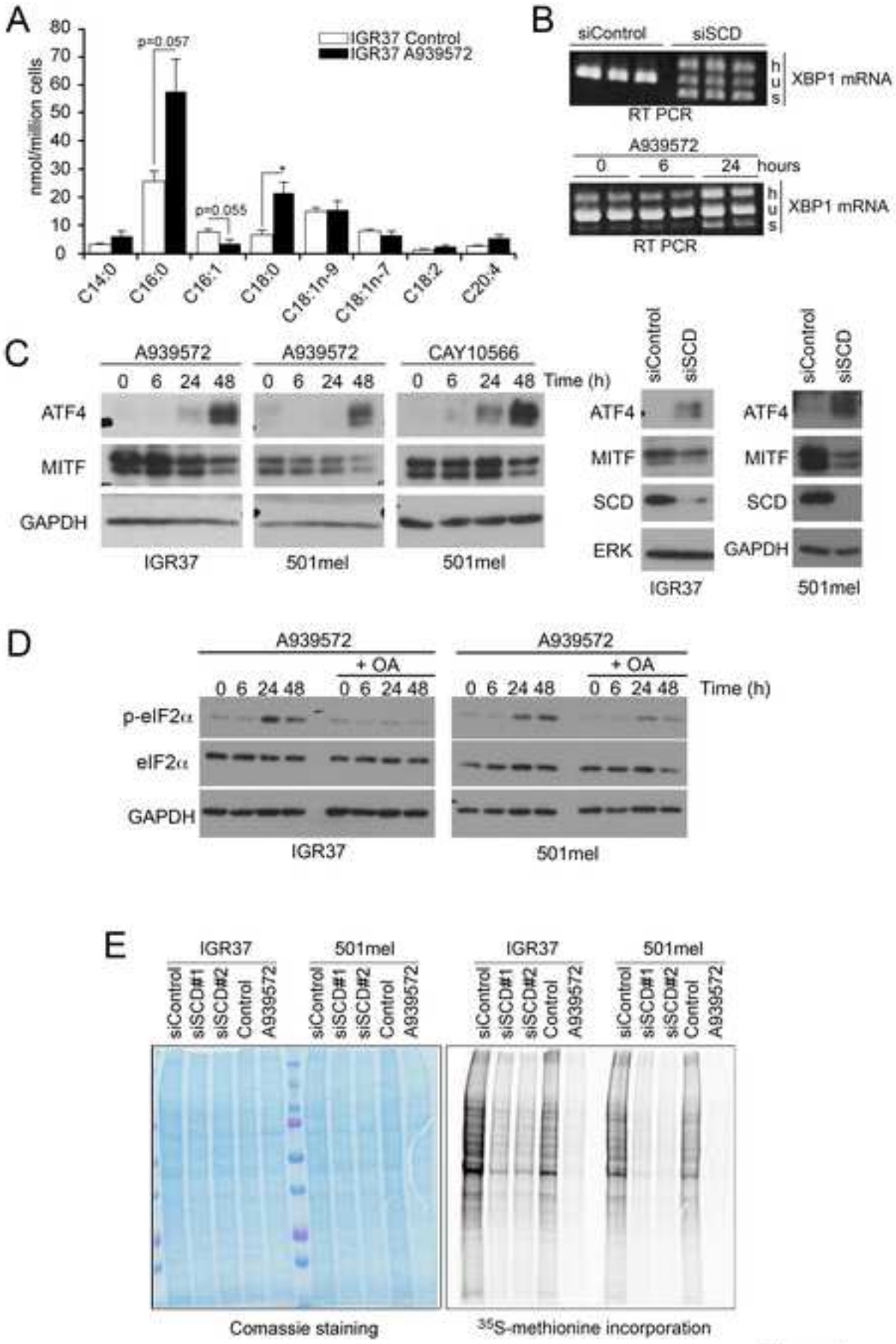

Figure 4

Figure 5

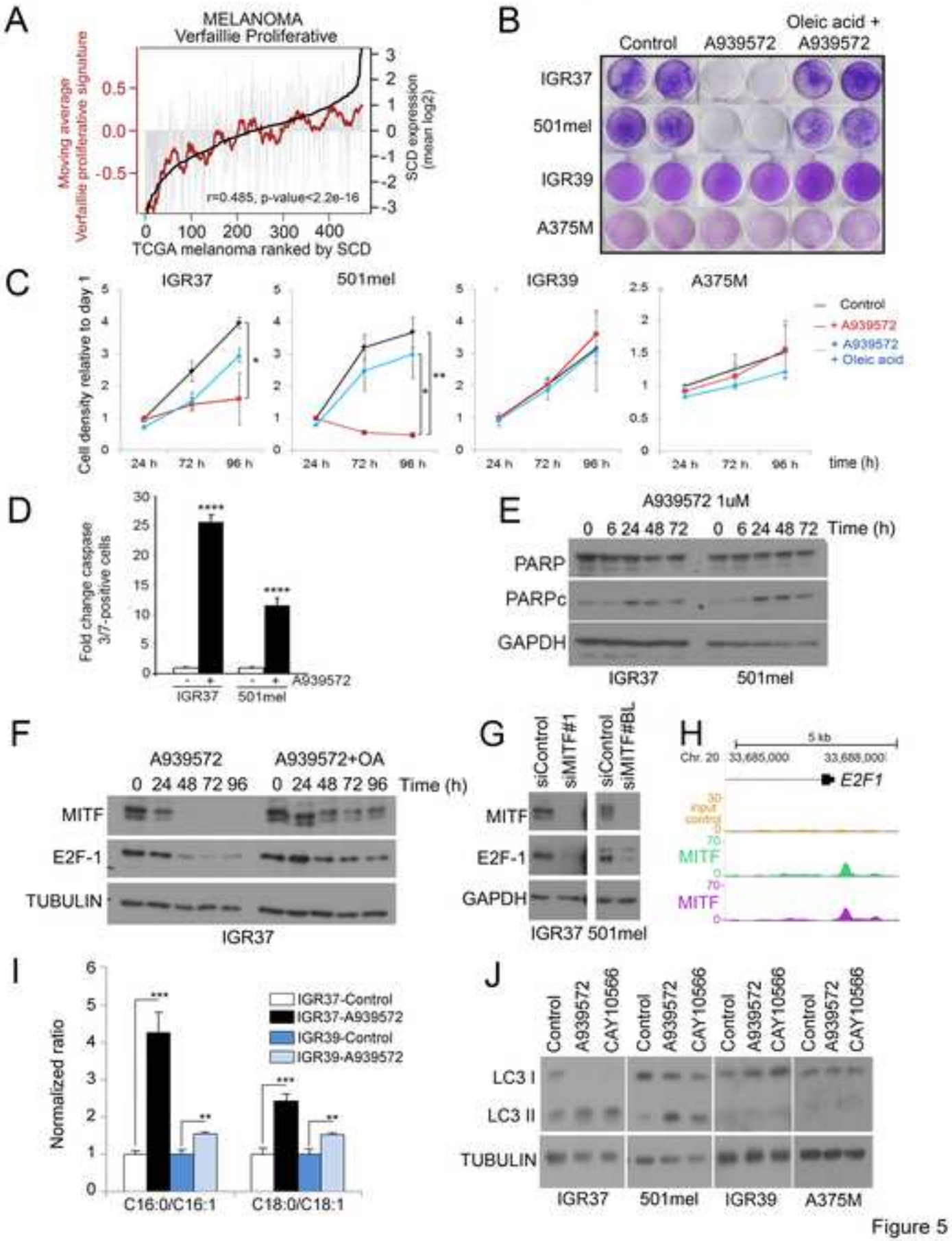

Figure 5

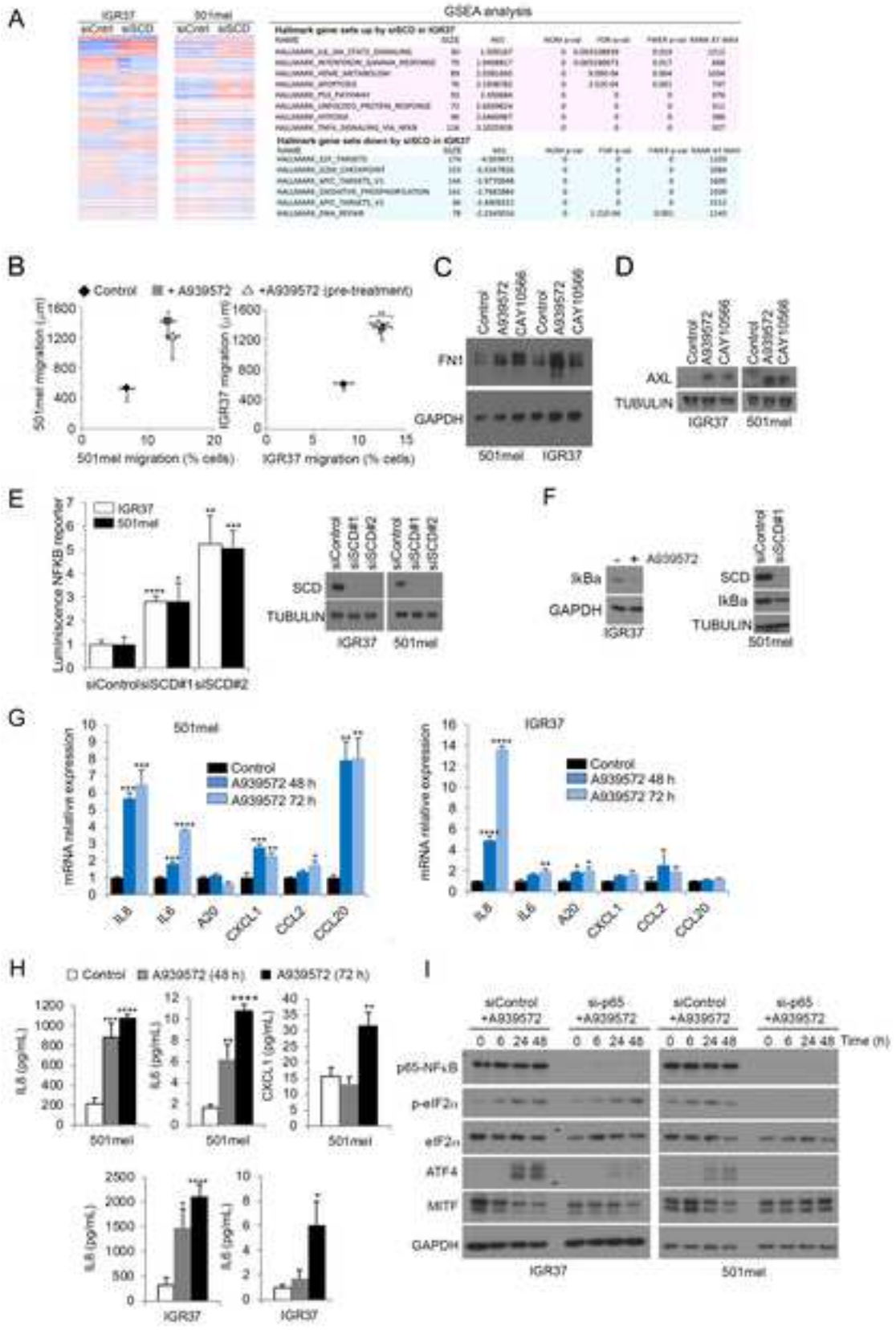

Figure 7

Click here to access/download;Figure;FIGURE 7SR.tif

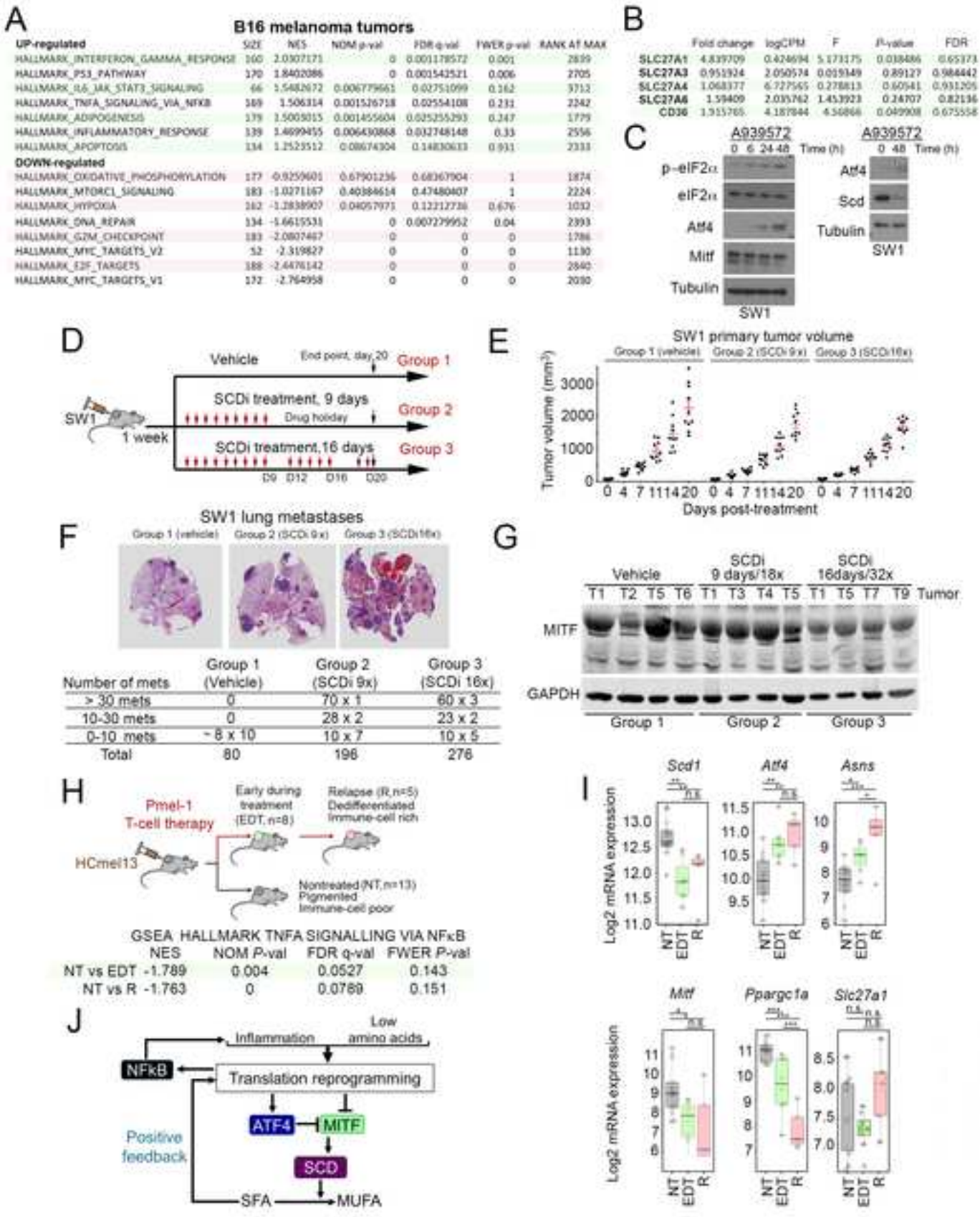

Figure 7

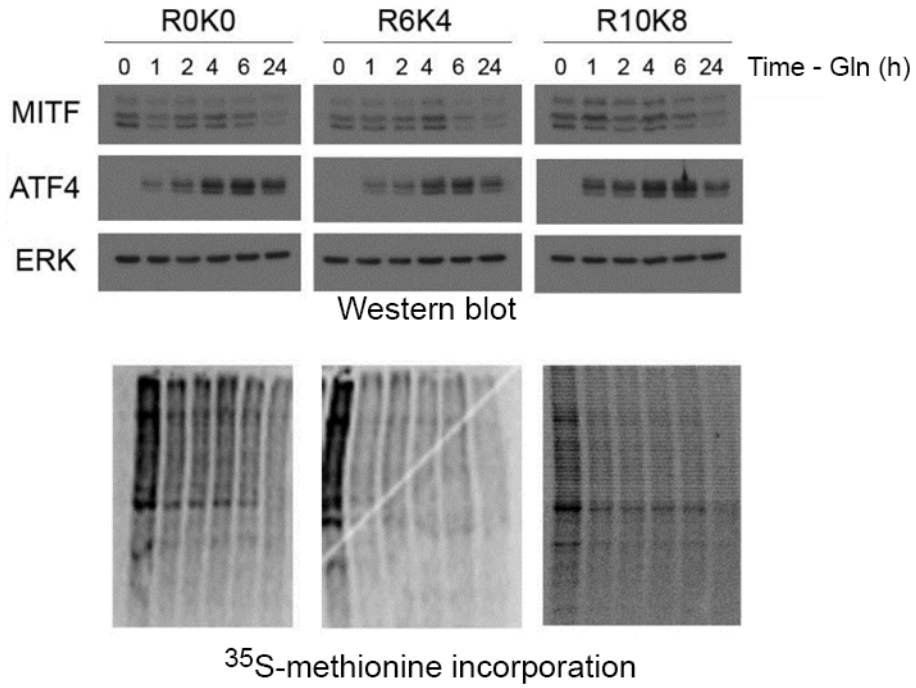

Figure S1 related to Figure 1A-C.

Translation reprograming was observed in samples analyzed by Stable isotope labelling with amino acids in cell culture (SILAC)

Upper panels. Western blot of IGR37 cells grown over time in SILAC DMEM without glutamine, showing MITF and ATF4 levels in three different populations of labelled cells: Light R0K0, Medium R6K4 and Heavy R10K8. ERK was used as a loading control.

Lower panels. ^{35}S-methionine labeling of IGR37 labelled cells (Light R0K0, Medium R6K4 and Heavy R10K8) grown over time in SILAC DMEM without glutamine.

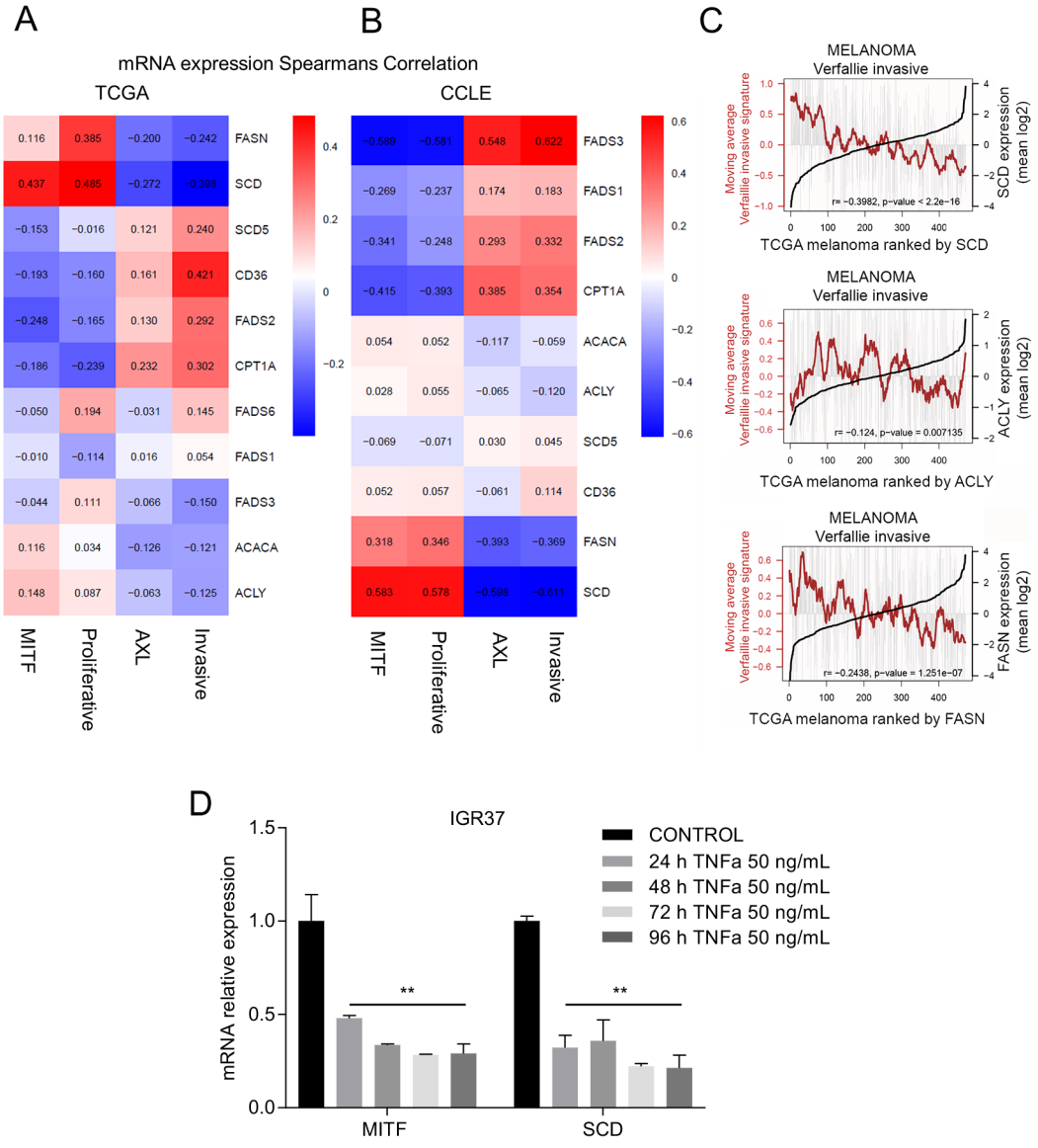

Figure S2 related to Figure 1.

SCD low expression correlates with a dedifferentiated phenotype in melanoma

(A, B) Heatmaps derived from gene expression data in the TCGA of CCLE databases showing correlations between indicated genes involved in fatty acid metabolism and MITF or the Verfaillie proliferative gene expression signature, or AXL (a hallmark of dedifferentiated drug-resistant melanoma) or the Verfaillie invasive gene expression signature.

(C) Correlation between Verfaillie invasiveness signature and SCD, ACLY or FASN. The 471 melanomas in the TCGA cohort were ranked by the SCD, ACLY or FASN expression (black line). Grey bars indicate expression of the SCD, ACLY or FASN in each of the tumors, and the brown line represents the moving average of Verfaillie invasiveness signature over each 20 tumors.

(D) RT qPCR from IGR37 cells showing expression of MITF and SCD mRNA in response to TNFα (50 ng/mL) at the indicated time. Data presented as mean +/- SEM. ** p <0.01.

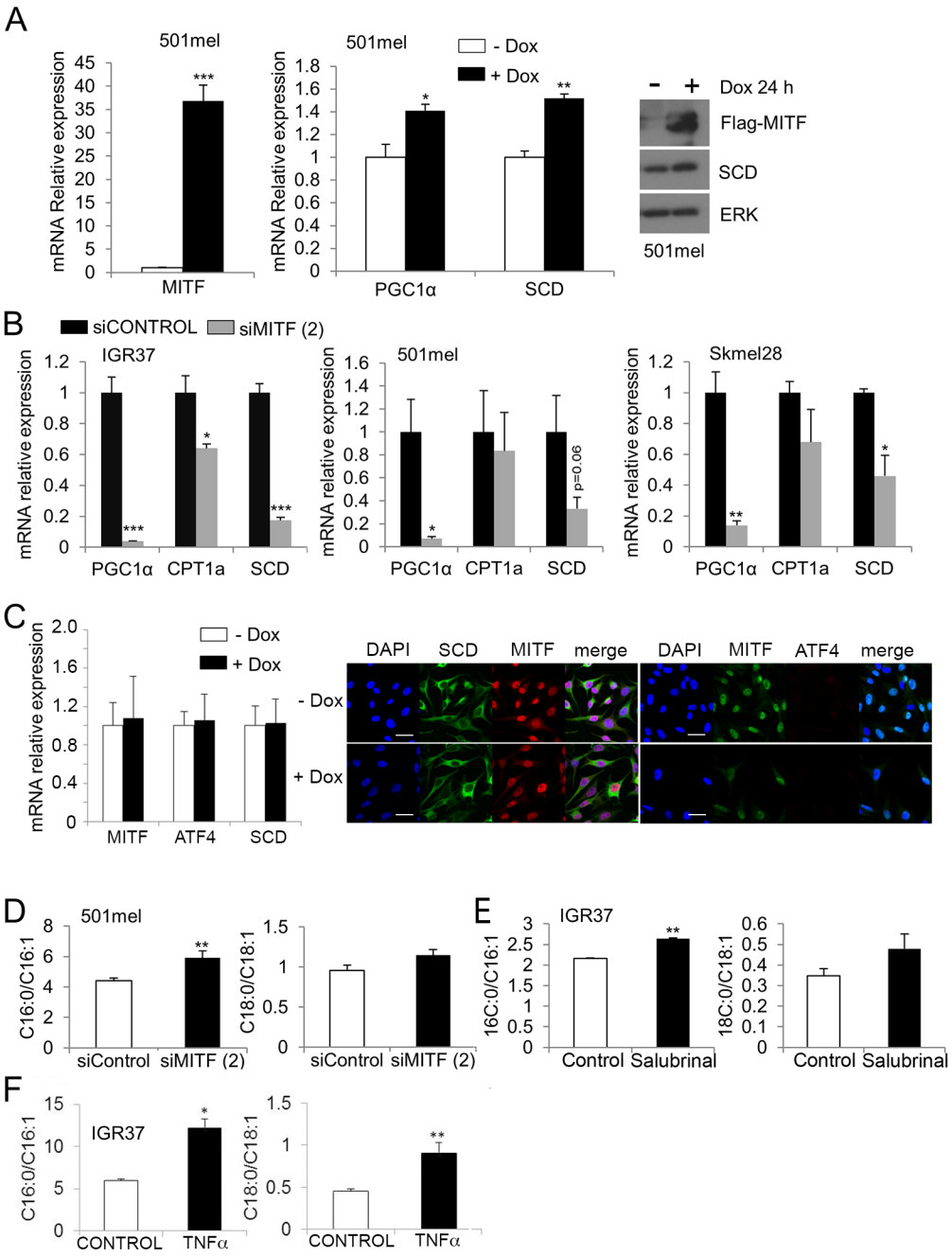

Figure S3 related Figure 3.
MITF regulates fatty acid desaturation in melanoma

(A) RT qPCR from 501mel cells expressing doxycycline-inducible MITF (iMITF) showing expression of MITF, SCD and PGC1α mRNA with or without doxycycline (100 ng/ml 24 h). A control western blot showing MITF induction as well as SCD expression using ERK as a loading control is shown to the right. Data are presented as mean +/- SEM. *$p < 0.05$; ** $p < 0.01$; *** $p < 0.001$

(B) RT qPCR from indicated cell lines cells transfected with control of siRNA targeting MITF. The known MITF target PGC1α was used as a positive control. Data are presented as mean +/- SEM. *$p < 0.05$; ** $p < 0.01$; *** $p < 0.001$

(C) RT qPCR and Immunofluorescence from 501mel parental cells grown during 24 h in the presence or absence of 100 ng/ml doxycycline as indicated. In the pictures, SCD (green), MITF (red or green) and ATF4 (no signal) are indicated. Scale bar = 20 μm.

(D) Results of GS-MS analysis showing relative levels of indicated saturated and monounsaturated fatty acids in 501mel cells transfected with control or MITF-specific siRNA. Data are presented as mean +/- SEM. ** $p < 0.01$.

(E) Results of GS-MS analysis showing relative levels of indicated saturated and monounsaturated fatty acids in Control IGR37 cells or treated with 50 μM salubrinal for 24 h . Data are presented as mean +/- SEM. ** $p < 0.01$.

(F) Results of GS-MS analysis showing relative levels of indicated saturated and monounsaturated fatty acids in Control IGR37 cells or treated with 50 ng/mL TNFα for 96 h. Data are presented as mean +/- SEM. *$p < 0.05$; ** $p < 0.01$.

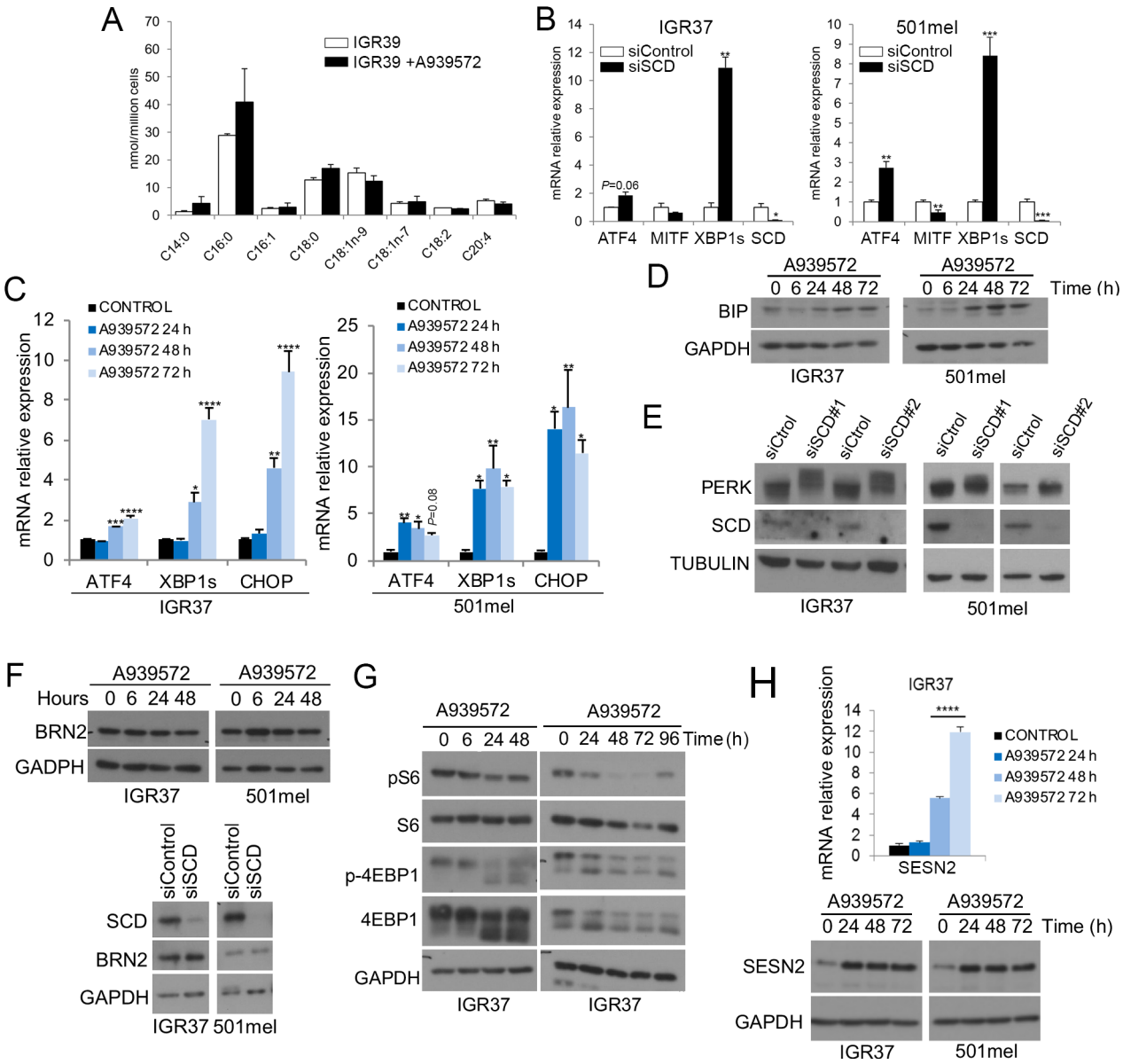

Figure S4 related to Figure 4.

Effects of SCD inhibition in melanoma cells

(A) Results of GS-MS analysis showing relative levels of indicated saturated and monounsaturated fatty acids in control IGR39 cells or cells treated with 1 µM A939572 for 48 h. Data are presented as mean +/-SEM.

(B) RT qPCR from indicated cell lines cells transfected with control of siRNA targeting SCD, showing effects on ATF4, MITF, XBP1s and SCD levels. Data are presented as mean +/-SEM. *$p < 0.05$; ** $p < 0.01$; *** $p < 0.001$.

(C) RT qPCR from IGR37 and 501mel cell lines treated with 1 µM A939572 at indicated time, showing effects on ATF4, XBP1s and CHOP mRNA levels. Data are presented as mean +/-SEM. *$p < 0.05$; ** $p < 0.01$; *** $p < 0.001$; **** $p < 0.0001$.

(D) Western blot for BiP on indicated cell lines exposed to 1 µM A939572 over time. GAPDH was used as a loading control.

(E) Western blot for PERK on IGR37 and 501mel cells transfected with control or two different SCD-specific siRNAs, showing band shift corresponding to phospho-PERK in response to SCD depletion. TUBULIN was used as a loading control.

(F) Western blot using anti-BRN2 antibody on indicated cell lines exposed to 1 µM A939572 over time of depleted for SCD using specific siRNA. GAPDH was used as a loading control.

(G) Western blot for phospho-S6, S6, phospho-4EBP1 and 4EBP1 on IGR37 cells exposed to 1 µM A939572 short term (up to 48 h) and long term (up to 96 h). GAPDH was used as a loading control.

(H) RT qPCR for SESN2 mRNA from IGR37 cells treated with 1 µM A939572 at indicated time. Data are presented as mean +/-SEM. **** $p < 0.0001$. Below, Western blot of IGR37 or 501mel cells treated for indicated times with 1 µM A939572. GAPDH was used as a loading control.

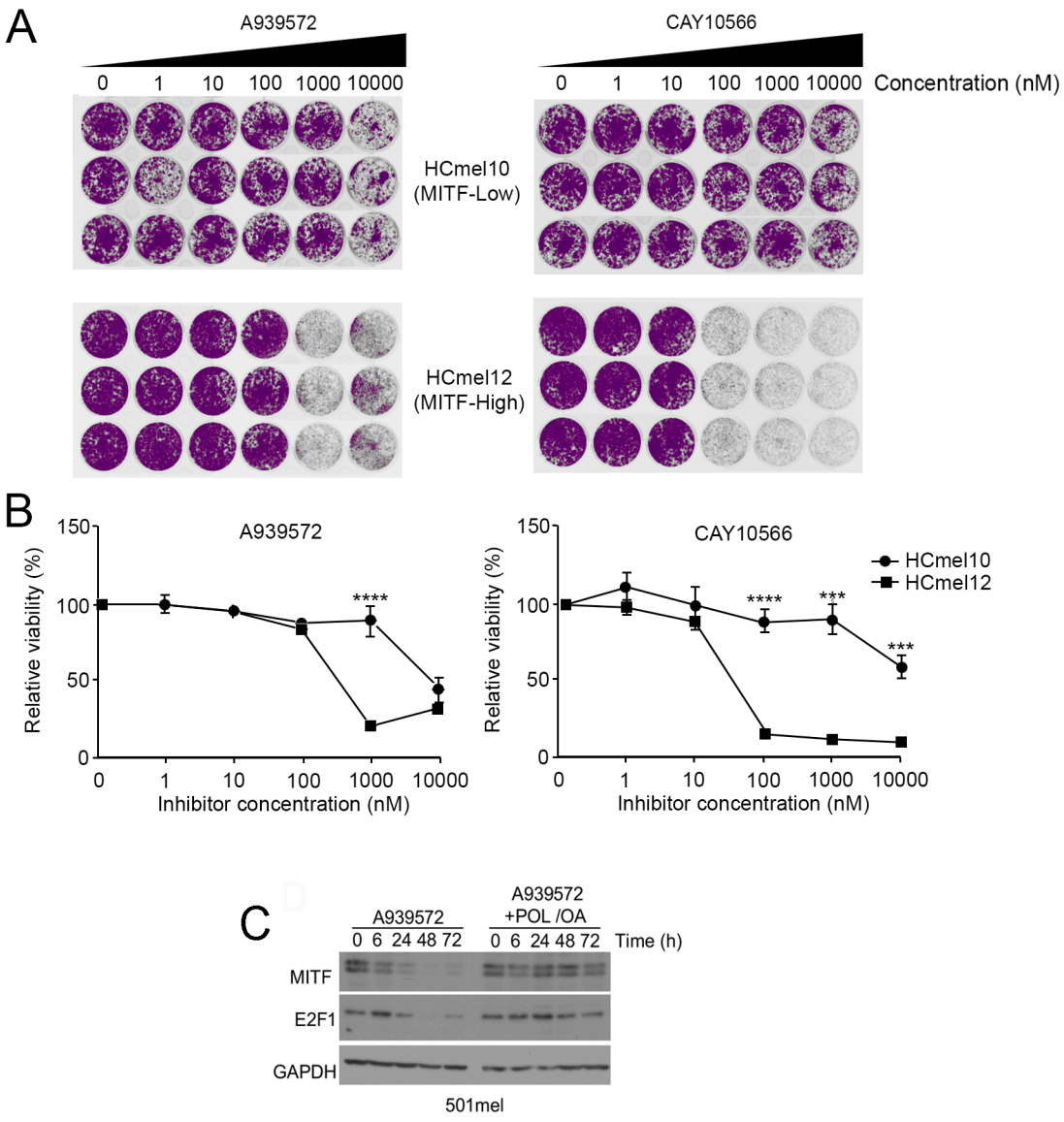

Figure S5 related to Figure 5.

(A) Indicated mice cell lines HCmel12 (MITF^{High}) and HCmel10 (MITF^{Low}) were grown for 6 days in a 12 well plate with or without different concentrations of A939572 or CAY10566 as indicated, before staining with 0.1% Crystal violet.

(B) Cell viability of indicated cell lines HCmel10 (MITF^{Low}) and HCmel12 (MITF^{High}) grown with indicated concentrations of A939572 or CAY10566. Quantification obtained from 0.1% crystal violet staining of three independent experiments. Data are presented as mean ± SEM. Statistics show differences between different treatments at each specific concentration. *** p <0.001; **** p <0.0001

(C) Western blot of 501mel cells showing MITF and E2F1 expression in response to SCD inhibition using 1 µM A939572, in the presence or absence of 50 µM oleic acid (C18:1) and 35 µM palmitoleic acid (C16:1). GAPDH was used as loading control.

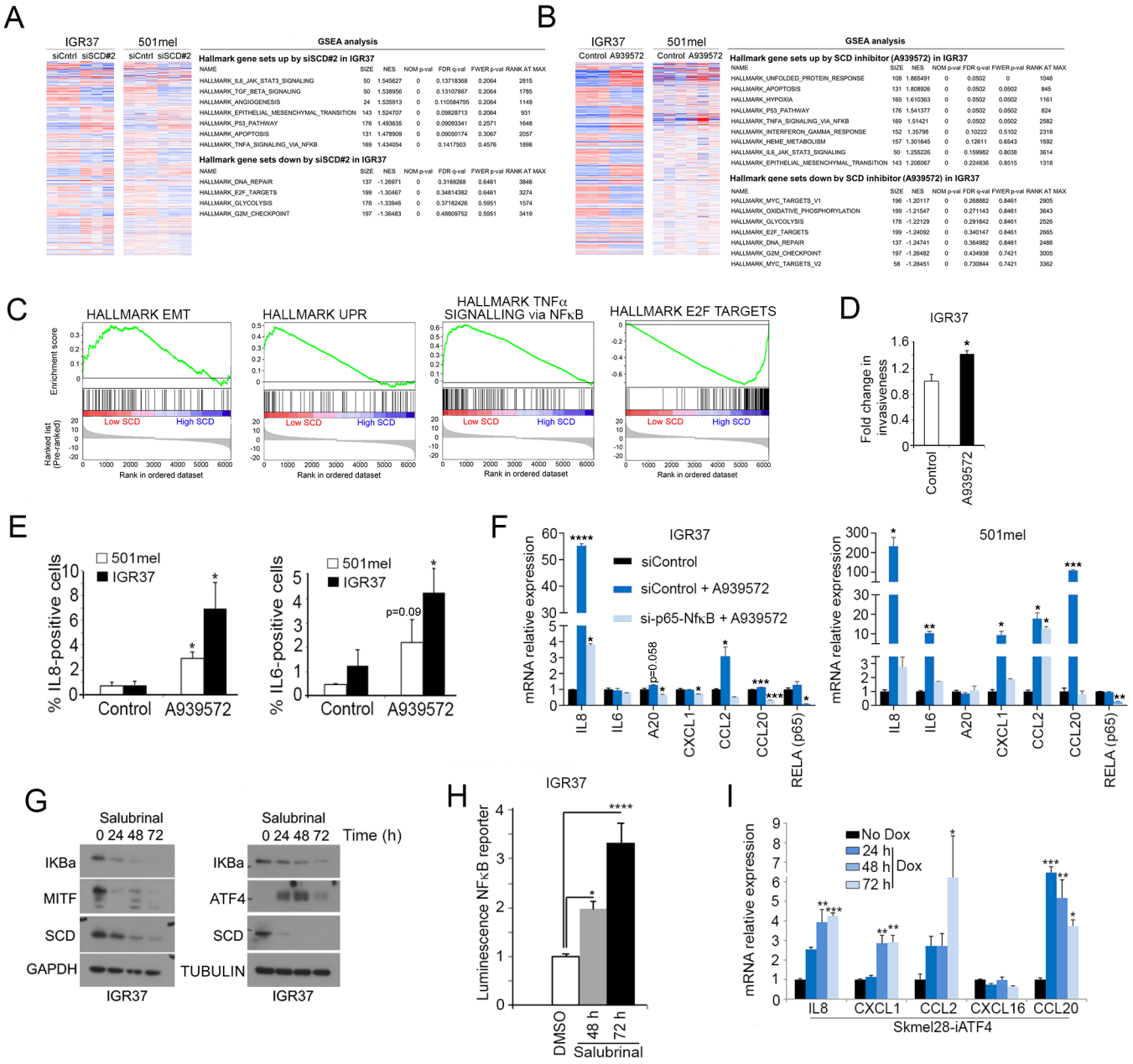

Figure S6 related to Figure 6.

SCD inhibition affects gene expression associated with inflammatory pathways, the UPR, the cell cycle and EMT-associated genes.

(A) Heatmaps and GSEA analysis derived from triplicate 3' RNA-seq of IGR37 or 501mel cells depleted for SCD with a second specific siRNA (siSCD#2).

(B) Heatmaps and GSEA analysis derived from triplicate 3' RNA-seq of IGR37 or 501mel cells treated with SCD inhibitor A939572 (1 µM) during 48 h.

(C) GSEA enrichment plots in IGR37 melanoma cells after 48 h of SCD silencing (siSCD#1). Represented hallmarks: EMT, unfolded protein response, TNFα signaling via NFκB and E2F targets. Green lines: enrichment profiles.

(D) Result of matrigel invasion assay showing relative invasion of IGR37 cells before or after treatment with 1 µM A939572 for 48 h. Data are presented as mean ± SEM. * p <0.05.

(E) Intracellular levels of IL8 and IL6 in 501mel and IGR37 cells treated with 1 µM A939572 for 72 h. Data are expressed as mean ± SEM of 4 different experiments. * p <0.05.

(F) RT qPCR of the indicated genes from IGR37 and 501mel cells transfected or not with specific siRNA-p65-NFkB and treated with 1 µM A939572 for 48 h or 72 h, as indicated. Data are presented as mean ± SEM * p < 0.05; ** p <0.01; *** p <0.001; **** p <0.0001

(G) Western blot of IGR37 cells showing IκBa, MITF, ATF4 and SCD expression in response to salubrinal (50 µM) at indicated times. GAPDH and TUBULIN were used as loading control.

(H) Luciferase assay of IGR37 cells transfected with an NFκB-dependent promoter-luciferase reporter and treated with salubrinal (50 µM) at indicated times. Data are expressed as mean ± SEM. * p < 0.05; **** p <0.0001.

(I) RT qPCR for indicated genes from Skmel28 cells expressing doxycycline-inducible ATF4 (iATF4) before or after treatment with 100 ng/ml doxycycline for indicated times. Data are presented as mean ± SEM * p < 0.05; ** p <0.01; *** p <0.001.

A

GSEA analysis

Hallmark gene sets up by SCD inhibitor (CAY10566) in HCmel12

NAME	SIZE	ES	NES	NOM p-val	FDR q-val	FWER p-val	RANK AT MAX
HALLMARK_TNFA_SIGNALING_VIA_NFKB	116	0.599188	2.5332165	0	0	0	1118
HALLMARK_CHOLESTEROL_HOMEOSTASIS	52	0.6033014	2.1710398	0	0	0	1099
HALLMARK_UNFOLDED_PROTEIN_RESPONSE	102	0.5135736	2.070742	0	0	0	724
HALLMARK_INTERFERON_ALPHA_RESPONSE	48	0.5777479	2.0606468	0	0	0	765
HALLMARK_INTERFERON_GAMMA_RESPONSE	98	0.4675942	1.9077334	0	3.98E-04	0.002	1062
HALLMARK_INFLAMMATORY_RESPONSE	63	0.50247955	1.8733453	0	7.13E-04	0.004	1456
HALLMARK_REACTIVE_OXIGEN_SPECIES_PATHWAY	36	0.5678437	1.8684531	0	6.24E-04	0.004	1066
HALLMARK_IL6_JAK_STAT3_SIGNALING	38	0.5146653	1.714241	0	0.00438508	0.035	557
HALLMARK_APOPTOSIS	107	0.4085268	1.6872978	0	0.005256862	0.047	842

Hallmark gene sets down by SCD inhibitor (CAY10566) in HCmel12

NAME	SIZE	ES	NES	NOM p-val	FDR q-val	FWER p-val	RANK AT MAX
HALLMARK_OXIDATIVE_PHOSPHORYLATION	175	-0.49931914	-2.3263674	0	0	0	1889
HALLMARK_G2M_CHECKPOINT	174	-0.40092194	-1.8770714	0	0.00326824	0.007	2222
HALLMARK_E2F_TARGETS	175	-0.38074368	-1.7878405	0	0.006068411	0.02	2504

B

GSEA plots HCmel12

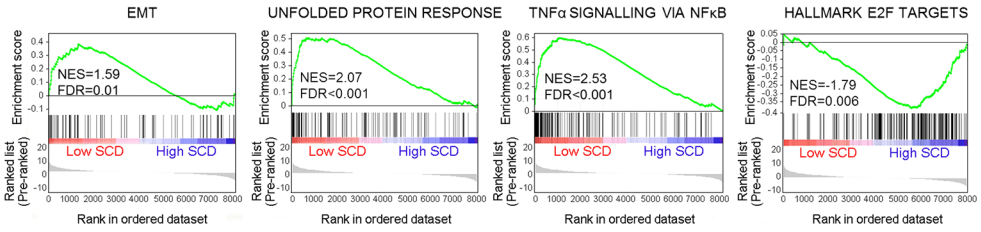

C

Hallmark gene sets up by SCD inhibitor (CAY10566) in B16

NAME	SIZE	ES	NES	NOM p-val	FDR q-val	FWER p-val	RANK AT MAX
HALLMARK_TNFA_SIGNALING_VIA_NFKB	116	0.60126054	2.5843878	0	0	0	987
HALLMARK_REACTIVE_OXIGEN_SPECIES_PATHWAY	36	0.61003214	2.0716016	0	0.001098276	0.002	769
HALLMARK_MYC_TARGETS_V2	54	0.4957796	1.8420078	0.001953125	0.009181221	0.026	2270
HALLMARK_INFLAMMATORY_RESPONSE	63	0.45785767	1.7795092	0.001941748	0.011310482	0.043	665
HALLMARK_IL6_JAK_STAT3_SIGNALING	38	0.51591444	1.7559903	0.007707129	0.010183534	0.048	1156

Hallmark gene sets down by SCD inhibitor (CAY10566) in B16

NAME	SIZE	ES	NES	NOM p-val	FDR q-val	FWER p-val	RANK AT MAX
HALLMARK_E2F_TARGETS	175	-0.39138106	-1.8247068	0	0.015730402	0.016	1855
HALLMARK_G2M_CHECKPOINT	174	-0.38389465	-1.7778839	0	0.012761436	0.026	1847

Figure S7 related to Figure 6A.

The effects of SCD inhibition on gene expression in mouse cell lines.

(A) GSEA analysis of triplicate 3' RNA-seq of HCmel12 mouse melanoma cells treated during 72 h with the SCD inhibitor CAY10566 (100 nM).

(B) GSEA enrichment plots in HCmel12 melanoma cells treated during 72 h with CAY10566 (100 nM). Represented hallmarks: EMT, unfolded protein response, TNFα signaling via NFκB and E2F targets. Green lines: enrichment profiles. Vertical black lines: Hits.

(C) GSEA analysis of triplicate 3' RNA-seq of B16 mouse melanoma cells treated during 72 h with the SCD inhibitor CAY10566 (100 nM).

Suppl. Table 1

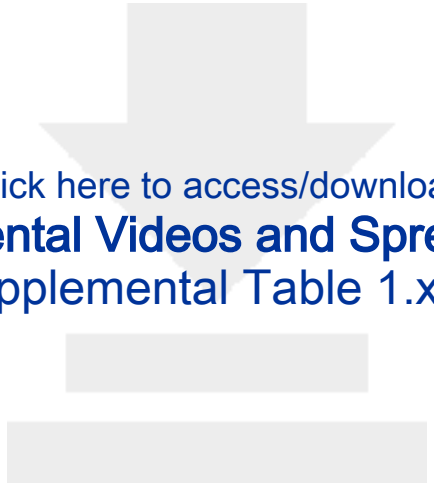

Click here to access/download

Supplemental Videos and Spreadsheets

Supplemental Table 1.xlsx

Suppl. Table 2

Click here to access/download

Supplemental Videos and Spreadsheets

Supplemental Table 2.xlsx

Suppl. Table 3

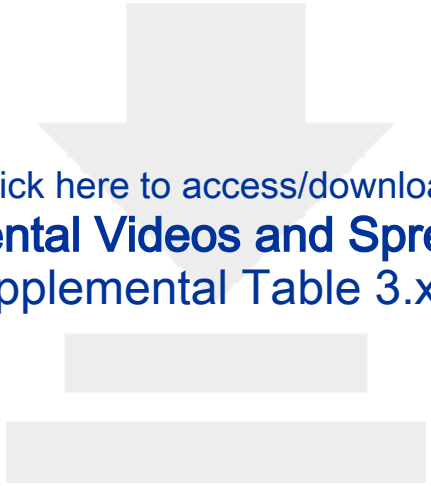

Click here to access/download

Supplemental Videos and Spreadsheets

Supplemental Table 3.xlsx

Suppl. Table 4

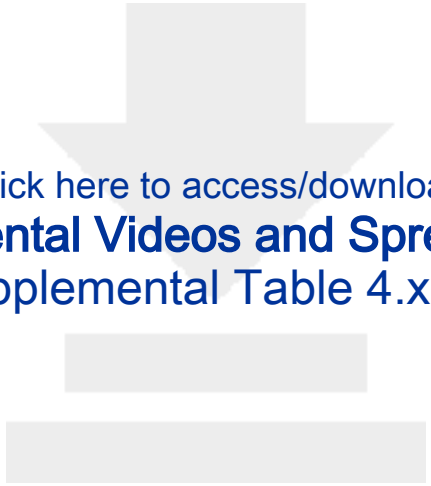

Click here to access/download

Supplemental Videos and Spreadsheets

Supplemental Table 4.xlsm

Suppl. Table 5

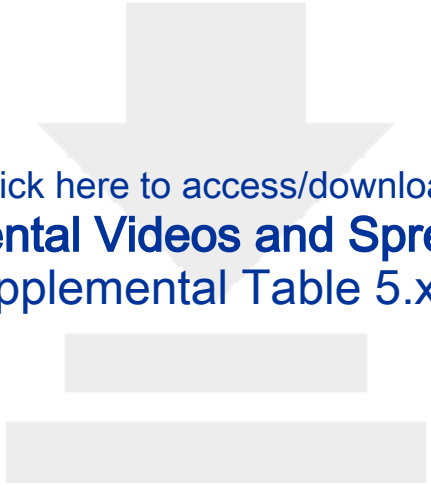

Click here to access/download

Supplemental Videos and Spreadsheets

Supplemental Table 5.xlsx

Suppl. Table 6

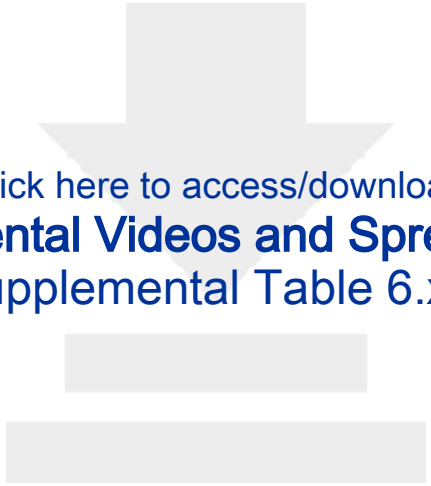

Click here to access/download

Supplemental Videos and Spreadsheets

Supplemental Table 6.xls